

**HOST-MICROBIOME INTERACTIONS AND
REGULATION OF THE IMMUNE SYSTEM**

by

CARLOS A. ALVAREZ CONTRERAS

Submitted in fulfillment of the requirements for the
Degree of Doctor of Philosophy

Thesis Advisor: Dr. Brian A. Cobb, Ph.D.

Department of Pathology

CASE WESTERN RESERVE UNIVERISTY

January 2021

CASE WESTERN RESERVE UNIVERSITY

SCHOOL OF GRADUATE STUDIES

We hereby approve the dissertation of

Carlos A Alvarez Contreras

Candidate for the degree of Doctor of Philosophy*

Committee Chair

Booki Min

Committee Member

Kristie Ross

Committee Member

Pushpa Pandiyan

Committee Member

Brian Cobb

Committee Member

Clive Hamlin

Date of Defense

August 3 , 2020

*We also certify that written approval has been obtained for any proprietary material contained therein

Dedication

I dedicate this to my family, friends, mentors and all the wonderful people I've met during my time here at CWRU. It is your friendship, guidance, support and love that has made this journey possible.

Table of Contents

List of tables.....	8
List of figures	9
Acknowledgements	12
List of abbreviations	13
Abstract.....	15
Chapter 1: The host-microbiome relationship and the impact on the immune response	
1.1 Introduction to the microbiome	18
1.2 Immune system recognition of the microbiome	21
1.3 Microbiome and disease	22
1.4 Pleiotropic effects of the immune-microbiome response.....	24
Chapter 2: Purification of Capsular Polysaccharide Complex from Gram Negative Bacteria	
2.1 Abstract.....	29
2.2 Introduction.....	29
2.3 Materials.....	31
2.3.1 Solutions, Reagents and Supplies	31
2.3.2 Special Equipment	33
2.4 Methods.....	34

2.4.1 Harvest and Phenol Extraction	34
2.4.2 Ether Extraction	35
2.4.3 Digestion and Precipitation	36
2.4.4 Chromatography	38
2.4.5 Fraction Analysis and Sample Pooling	38
2.4.6 Quality Check	39
2.4.7 Storage	39
2.5 Notes	40
 Chapter 3: CD45Rb-Low Effector T Cells Require IL-4 to Induce IL-10 in FoxP3 Tregs and to Protect Mice from Inflammation	
3.1 Abstract.....	47
3.2 Introduction.....	48
3.3 Methods.....	50
3.3.1 Mice.	50
3.3.2 Primary splenic T cells.	50
3.3.3 Pulmonary inflammation and adoptive transfer.	51
3.3.4 Flow cytometry and cell sorting	51
3.3.5 Cell culture.	52
3.3.6 ELISA, blocking, supplementation and Luminex.	52
3.3.7 RNAseq and analysis.	53
3.3.8 Histology and microscopy.	54
3.3.9 Clinical Scoring.	54

3.3.10 Data analyses.	55
3.3.11 Data availability.	55
3.4 Results	55
3.4.1 Rb ^{Lo} Tem cells induce IL-10 in FoxP3 ⁺ Tregs	55
3.4.2 IL-10 synergy is unique among common cytokines	57
3.4.3 IL-10 synergy depends on a soluble mediator	58
3.4.4 The Rb ^{Lo} Tem transcriptome	60
3.4.5 Neutralization of IL-4 eliminates IL-10 synergy	60
3.4.6 Rb ^{Lo} Tem cells require IL-4 to protect mice from pulmonary inflammation.....	62

Chapter 4: Characterization of Polysaccharide A Response Reveals Interferon
Responsive Gene Signature and Immunomodulatory Marker Expression

4.1 Abstract.....	75
4.2 Introduction.....	76
4.3 Methods.....	78
4.3.1 Mice	78
4.3.2 PSA Purification	79
4.3.3 Primary Splenic, Peyer's Patch and Mesenteric Lymph Node T Cells	79
4.3.4 Flow Cytometry and Cell Sorting	79
4.3.5 Cell Culture	80
4.3.6 ELISA, Blocking, Supplementation and Luminex	80
4.3.7 RNAseq and Analysis	81

4.3.8 Data Analyses	81
4.4 Results	81
4.4.1 PSA-activated T cells show transcriptomic changes consistent with clonal expansion	81
4.4.2 PSA-responding T cells show an Interferon Responsive Gene (IRG) signature	83
4.4.3 PSA-responding T cells show Th1-skewed signaling molecule and transcription factor expression	84
4.4.4: Protein levels in PSA-responding T cells are consistent with an IRG signature	84
4.4.5: PSA-associated co-regulatory receptors are IRGs	86
4.4.6: Co-regulatory receptors are increased within the GALT of PSA- exposed mice	87
Chapter 5: Discussion and future directions	98

List of Tables

Chapter 3: CD45Rb-Low Effector T Cells Require IL-4 to Induce IL-10 in FoxP3

Tregs and to Protect Mice from Inflammation

Table 1. Lung inflammation clinical score rubric63

List of Figures

Chapter 2: Purification of Capsular Polysaccharide Complex from Gram Negative Bacteria

- Fig. 1 Phenol extraction assembly for the initial extraction of LPS and capsular polysaccharide from intact gram-negative bacteria.44
- Fig. 2 Pro-Q Emerald stained SDS-PAGE gels from the purification of PSA from *B. fragilis*.45

Chapter 3: CD45Rb-Low Effector T Cells Require IL-4 to Induce IL-10 in FoxP3 Tregs and to Protect Mice from Inflammation

- Figure 3. IL-10 production by Tregs is synergistically enhanced by CD4⁺FoxP3⁻ CD45Rb^{Lo}CD44⁺CD62L⁻ T cells64
- Figure 4. Cytokine synergy of Rb^{Lo}Tem and FoxP3⁺ Tregs is limited to IL-10..65
- Figure 5. T cell synergy is mediated by a soluble factor66
- Figure 6. Rb^{Lo}Tem and Rb^{Hi}Tn transcriptomes reveal potential crosstalk mediators67
- Figure 7. IL-4 and FoxP3⁺ Treg IL-4R α (CD124) mediates Treg IL-10 production.....68
- Figure 8. Rb^{Lo}Tem cells reverse lung inflammation in an IL-4-dependent fashion69

Figure 9. Lung inflammation, remodeling and mucus production is reversed by Rb ^{Lo} Tem cells in an IL-4-dependent fashion	70
Figure 10. Flow setup for sorting Tregs based on CD25	71
Figure 11. Flow setup for sorting T cell subpopulations	72
Figure 12. Blocking neuropilin1 does not engage IL-10 production in Tregs ..	73

Chapter 4: Characterization of Polysaccharide A Response Reveals Interferon

Responsive Gene Signature and Immunomodulatory Marker Expression

Figure 13. Gene enrichment and ontology analysis in response to PSA exposure.....	89
Figure 14. Gene set enrichment analysis of inflammatory and interferon related genes.....	90
Figure 15. Gene expression IRG signature of PSA exposed cells.....	91
Figure 16. Transcription factor and signaling molecule profile of PSA exposed cells	92
Figure 17. Secreted molecule profile of PSA exposed cells	93
Figure 18. Unchanged cytokines and chemokines in PSA-exposed cell culture	94
Figure 19. Cell surface marker expression of PSA exposed CD4 ⁺ T cells identifies immunomodulatory markers	95
Figure 20. IFN-γ influence on immunomodulatory marker expression.....	96

Figure 21. Gut associated lymphoid tissue enrichment of PSA induced markers
.....97

Acknowledgements

Thank you to everyone in my life who has supported me before and during this process.

To all the friends I have made during my graduate career, sharing our triumphs, frustrations and losses have helped keep me afloat during times of isolation.

Thank you to my lab members (past and present) Doug, Julie, Kelsey, Mark, Jill, Lori, Eddie, Eli, Emily and Kalob. I have learned more by interacting and working with all of you than ever before. Beyond science, you have all been an integral component in making my time in lab a happy one. As of one of you once said, it's not the work but the people that make it worthwhile.

To my PI and mentor Brian Cobb, you are truly a paragon of what a mentor should be. Continuously supportive, patient, knowledgeable yet approachable, I have learned much from you both in and out of science.

Thank you to my committee members Dr. Pushpa Pandiyan, Dr. Kristie Ross, Dr. Clive Hamlin and Dr. Booki Min for your continued support and guidance.

To my family, who continues to support me regardless of my endeavors.

And to my girlfriend Hannah, you have changed my life in many ways. I am thankful to have found such a loving and thoughtful individual such as yourself.

You make me want to be a better person, thank you.

List of Abbreviations

APC: Antigen Presenting Cell

BALF: Broncho alveolar lavage fluid

CRA: Cockroach antigen

DEG: differentially expressed genes

EAE: experimental autoimmune encephalomyelitis

EDTA: Ethylenediaminetetraacetic acid

ELISA: enzyme linked immunosorbent assay

EpCAM: Epithelial cell adhesion molecule

FDR: False discovery rate

GALT: Gut associated lymphoid tissue

GeoMFI: Geometric mean fluorescence

GO: Gene ontology

GSEA: Gene set enrichment analysis

HDM: House dust mite

H&E: Hematoxylin and eosin

IBD: Inflammatory bowel disease

IL-: Interleukin

IL-10^{-/-}: IL-10-deficient

IL-4ko: IL-4 knockout

IN: Intra nasal

IRG: Interferon responsive gene

LPS: Lipopolysaccharide

MDS: Multi-dimensional scaling plot

MHCII: Major histocompatibility complex class II

MLN: Mesenteric lymph nodes

MPO: Myeloperoxidase

NLR: NOD like receptor

OVA: Ovalbumin

PAS: Periodic Acid-Schiff

PP: Peyer's Patch

PSA: Polysaccharide A

PSB: Polysaccharide B

PBS: Phosphate buffered saline

RNAseq: mRNA deep sequencing

RPKM: Reads per kilobase of transcript, per million mapped reads

STAT: signal transducer and activator of transcription

Tconv: Conventional T cells

Tem: CD4⁺ effector/memory T cells

Th1: T helper cell type 1

Treg: Regulatory T cells

Tr1: Type 1 regulatory cells

TLR: Toll like receptor

TNFR: Tumor necrosis factor receptor

WT: Wild type

Host-microbiome interactions and regulation of the immune system

Abstract

by

CARLOS ALBERTO ALVAREZ CONTRERAS

Multifactorial diseases such as diabetes, allergy and asthma, inflammatory bowel disease and neurodegenerative disorders have increased in recent years.

Genetic predisposition is unable to fully account for this sudden increase, yet our environment is a factor that has seen similar dramatic changes even in the last 100 years. It has since become apparent that the gene pool of endogenous microbes that populate our bodies might be more susceptible to these changes due to their shorter life span and generation turnover. Thus, examination of the microbiome has become a major focus in the hopes of identifying underlying changes in the microbiome which may give rise to or be compounded due to disease. Study of these interactions have revealed the involvement of the microbiome in many functions ranging from processing of nutrients, neuronal and immune system development.

The host immune interactions with gut commensal microbes have demonstrated their importance in establishing tolerance and maintenance of homeostasis.

Here, we utilized the capsular polysaccharide PSA produced by the gut commensal *Bacteroides fragilis* to better understand the impact on the host immune system locally and systemically.

Prior work established that PSA is endocytosed, processed and presented by APCs to CD4⁺ T cells via MHCII molecules. This exposure lead to the expansion of a population of C45Rb^{low} effector memory (Tem) cells capable of protecting from induction of inflammation. This protection was shown to be IL-10 dependent, the source of which was endogenous Tregs and not the PSA expanded cells. Through *in vitro* co-culture experiments with regulatory T cells, we demonstrated a novel T cell communication axis by which Tem cells secrete IL-2 and IL-4 to synergistically stimulate IL-10 production by Tregs. Furthermore, we demonstrated that PSA exposure results in potent interferon response, which results in the upregulation of immune-regulatory markers. These markers were primarily found in the gut associated lymphoid tissue, providing an example by which commensal microbiota exposure can directly impact the immune cell population.

Understanding how the host-microbiome interactions can impact the immune response can help in the treatment development and therapeutics for multiple inflammatory diseases.

**Chapter 1: The host-microbiome relationship and the impact on the
immune response**

1.1 Introduction to the microbiome

In the early 2000s, the completion of the human genome project allowed the opportunity for scientists to dissect the all genes contained within the human body. The data collected has been used to develop tools and technology for diagnosing, treating and preventing human disease[1]. However, this has only been accomplished by expanding our understanding beyond the genome of an organism. Study of the proteome has helped to identify and categorize thousands of proteins[2], while the epigenome has uncovered regulatory mechanism that govern the accessibility and transcription of genes[3, 4]. An additional factor has been recognized as crucial and dynamic in its ability to regulate human health, the human microbiome.

Within our bodies there is exists a rich and diverse community of bacteria, fungi, protozoans and viruses, and the metagenome of these microorganisms is collectively referred to as the microbiome[5]. The microbiome has co-evolved with the host's own genome, developing a delicate but profound symbiotic relationship. These microbes colonize major intersection between our body and our environment, namely the skin, oral cavity, airways, gastrointestinal tract, urogenital and ocular surfaces[6-10].

Attempts aiming to classify the diversity of the healthy microbiome to establish a conserved core set of microbial taxa to be used as a reference to then identify unhealthy states, allowing them to be linked to disease[5]. Similar to reference

genomes of the human genome project[11] , it was quickly discovered that no conserved pattern throughout every single individual could be used as a clear determinant of health or disease[12, 13]. There is inherent variation in taxonomic composition depending on the location on the body, the surrounding environment, dietary intake and even the interactions with other individuals. The microbiome has been selected for function rather than composition, discarding or replacing taxa as needed in order to better adapt to the current environment and needs of the host[14, 15]. The composition of the skin microbial community varies depending on the characteristics of the skin site. Hairy and moist areas harbor different microbial communities compared to dry and smooth regions[16]. Other areas remain elusive in terms of their microbial composition, namely human breast milk which has been shown to provide nutrients and bacteria for the initial seeding of a healthy microbiome in infants. The relatively low biomass, inconsistencies and contamination during sample collection have hindered the study of such a critical component of human biology[17-19].

The collection, culture and identification of the components of the microbiome have undergone many changes over recent years. Out of all the components of the microbiome, the bacterial components have been the most studied and best understood. The introduction of advanced culturing techniques such as anaerobic and selective media, along with the accessibility to 16s RNA and high throughput sequencing technology have allowed for detailed identification of bacterial, fungal and viral component present in the microbiome of different

organs. These techniques have only served to highlight the inherent richness of the microbiome, an example being the reclassification of the species that once belonged to *Bacteroides* into 5 distinct genre: *Alistipes*, *Prevotella*, *Paraprevotella*, *Parabacteroides* and *Odoribacter* [20]. Limitations in terms of sample collection, purity, analysis and standard comparisons need to be overcome to gain better understanding of the microbiome across all areas of the body.

Several terms have surfaced in an attempt to accurately describe a healthy microbiome. A “healthy core” incorporates the molecular functions provided by the microbial population that otherwise are not provided by the host, while maintaining vital transcription and translation functions needed for the microbial community to survive. Additionally, the inclusion of mechanism necessary for colonization are required if any stability is to be achieved[21]. This supports the idea of favoring common pathways and molecular functions needed for survival in the microbiome which might be fulfilled by a variety of microbes[15].

Carbohydrate processing and harvesting by oral microbes[22], release of antimicrobial peptides and protection from invasive species in the skin[23], fermentation and degradation of polysaccharides in the gut [13], and production of organic acids and maintenance of pH in the vagina[9, 24] are examples of some of the functions attributed to a healthy microbiome.

The stability of the microbiome over time, its ability to resist or recover from both external and internal factors without developing disease phenotypes might be used to characterize a healthy microbiome[25]. The richness or diversity of the

human microbiome can also be as a determinant of health, although this could be easily misinterpreted when comparing samples[26]. An incorporation of all factors, and possibly others that have yet to be determined will continue to help define the concept of a healthy microbiome and lead to development of diagnostics and treatment for disease.

1.2 Immune system recognition of the microbiome

The relationship between the immune system and the microbiome is one of the most influential mechanisms by which health can be maintained or disease can arise.

Host and microbiome have co-evolved for mutual gain, developing regulatory and feedback mechanisms needed to maintain homeostasis. Several studies have shown innate and adaptive immune signaling is vital for surmounting an effective response against pathogens and maintaining a healthy microbiome population.

Pattern recognition receptors such as TLRs play a crucial role in sensing conserved molecular pattern such as LPS and peptidoglycan for the induction of innate immunity against potential pathogens[27]. Alteration of these sensors either by using TLR knockouts or removing key molecules involved in TLR signaling like MyD88 results in dysregulation of commensal bacteria and inflammation. It was determined that commensal bacteria in the gut are recognized by TLRs and are vital for the maintenance of gut epithelial cell homeostasis, protection from injury and proliferation of epithelial cells [28, 29].

The gut commensal *Bacteroides fragilis* requires TLR2 signaling for colonization,

activation of CD4⁺ T cells and immune-regulatory effects[21]. Similarly, NLRs have been shown to be necessary for the induction of intestinal lymphoid follicles and B cell recruitment, that when altered result in abnormal bacterial growth[30]. C-type lectins such as Dectin-1 have also been associated with regulation of the microbiome. Dectin-1, which recognizes β 1-3 glucans found in cell walls of most fungi, was shown to be necessary for regulating the fungal population in the gut. Dectin-1 deficiency resulted in pathogenic fungal infections and susceptibility to colitis[31].

In the absence of B cells or IgA production, gut microbiota induce upregulation of interferon inducible genes in epithelial cell as a compensatory mechanism, shifting the microbial population. This in turn leads to lipid malabsorption and fat loss[32]. T follicular helper cells with PD-1 deficiencies were shown dysregulate the production of IgA necessary for regulation of gut microbiota[33].

Lastly, it was demonstrated that polysaccharide components of commensal bacteria capsules are processed and presented via APC mediated MHCII molecules to CD4⁺T cells, resulting in an expansion of immune-regulatory cells[34, 35].

It is clear that a communication axis between tissue, microbiome and immune system is necessary and tightly regulated for maintenance of homeostasis.

1.3 Microbiome and disease

First proposed by the hygiene hypothesis, exposure to bacteria early in life could promote health and decrease incidence of disease later in life. Alternatively, a

lack of exposure can lead to an increase in disease[36]. When first proposed, the mechanism by which these microbes exerted their influence on the immune system were poorly understood. Since then, several studies have examined the factors that influence the establishment and maintenance of a healthy immune-microbiome relationship.

Commonly defined as a compositional or functional alterations of the microbiome relative to healthy individuals, dysbiosis became a focal point for understanding the relationship between disease phenotypes and microbial composition.

Dysbiosis has been connected to obesity[37], diabetes[38], IBD[39], and dermatitis[40] and multiple sclerosis[41] to name a few. Dysbiosis has been consistently shown to play major role in disease, yet the traditional definition of dysbiosis offers a limited understanding of the underlying mechanisms.

Studies across varied geographical, nutritional and ethnic communities have demonstrated the immense variability present in healthy individuals without any disease phenotype[13, 42]. Selecting any one group of healthy individuals as a “control population” might lead to false categorization of dysbiotic states. The same concern over comparing animal studies across facilities that have a wide range of living conditions, diets and maintenance has been the bane of modern science in terms of rigor and reproducibility[43].

Additionally, a change in composition by the microbiome in order to adapt to a change in environment might be a beneficial and necessary change compared to a previous steady state. Only when a chronically persistent perturbation is

maintained even when the environmental change is removed can it lead to detrimental consequences[44, 45].

Clinical and animal model data have elucidated common features associated with dysbiosis such as the bloom of pathobionts, opportunistic bacterial strains that may give rise to inflammation and disease[46]. The loss of commensals and overall diversity in the microbiome have been tied to dysbiosis, both of which might arise from similar circumstances such as exposure to xenobiotics and changes in diet, which in turn might lead to a bloom of opportunistic pathobionts[47-49].

One of the most detrimental factors involved in dysbiosis is inflammation and the loss of its regulation by the immune system. In mouse models of human diarrheal pathogens and infection using *Citrobacter rodentium*, it was shown that the hosts immune response resulted in the loss of endogenous commensal bacteria. In the same study it was demonstrated that use of IL10 KO mice which were prone to inflammation resulted in spontaneous colitis, and that it had impacted the growth of endogenous bacteria in favor of recently introduced species[50]. In this way the hosts own immune response designed to protect against pathogens results in the promotion invasive growth and increase in inflammation[51].

1.4 Pleiotropic effects of the immune-microbiome response

The concept of pleiotropy in immunology has long caused controversy when new roles for a studied molecule or process are discovered. Cytokine pleiotropy is perhaps the most recognizable application of this concept, in which a single

cytokine mediator can result in many different context dependent responses. Cell type, tissue type, injury, and inflammation can have drastic effect on the type of response. Similarly, the host-microbiome interaction can have many pleiotropic effects.

Interferons are a broad family of cytokines that play vital roles in the innate and adaptive response. Interferons are grouped into 3 different types, each with shared functions, signaling molecules but distinct context dependent roles. Type I IFNs compose a large group, but are generally responsible for surmounting antiviral responses, increasing antigen presentation, chemokine release and immune cell recruitment[52]. However, it has been shown that sustained IFN production leads to induction of suppressive dendritic cell programming, increases in PD-1 and IL-10 production, supporting viral infection while shutting down the ongoing immune response[53-56].

It has now been that gut microbiota are able to induce production of type 1 IFNs in order to establish activation thresholds for the immune system, important for hematopoietic cell maintenance, autoimmunity and cancer[57, 58]. Similar microbiota and IFN dependent effects have been shown to be important in regulating epithelial cell hyper proliferation and tumor burden[59].

Understanding how the immune system responds to dysbiosis and disease can lead to development of strategies to correct or compensate for these mechanisms.

1.5 Microbiome mediated immune modulation

Some studies have been able to delve into the mechanisms by which microbes and their metabolites can exert immune modulatory effects.

When examining patients with Celiac disease, an imbalance between the full length FoxP3 and its isoform were found that affected regulatory T cell's ability to downregulate ROR γ T and IL17A. Stimulation PBMCs with IFN γ and microbial derived butyrate a balance between both FoxP3 forms was attained, while microbial derived lactate also increased expression of both versions of FoxP3[60]. Gut bacteria are able to utilize soluble fibers to produce short chain fatty acids, which have been shown to activate TNF- α secretion in M2 macrophages, promote the development of IL-10 secreting Tregs, Th1, Th2 and Th17 with suppressive properties[61].

Bacteroides fragilis and its primary immunomodulatory metabolite polysaccharide A(PSA) exemplify the pleiotropic nature of the immune-microbiome response. Identified as the most common isolate in abscesses in human with bacteremia, it was quickly discovered that immunization with its capsular polysaccharide protected from abscess formation[62, 63]. Of the 8 capsular polysaccharides, PSA has been studied to a large extent due to its potent immunomodulatory effects. PSA is comprised of a tetrasaccharide repeating units which form an extended right handed helix with positive one positively charged amine and one negatively charged carboxylate [64]. It is this zwitterionic motif that was shown to be crucial for the interaction with MHCII and subsequent presentation to CD4⁺ T

cells. Both *B. fragilis* and purified PSA have been shown to protect against IBD, EAE and asthma induction[35, 65-67]. PSA exposure has since been shown to expand a population of T effector memory cells capable of inducing IL-10 secretion on endogenous regulatory T cells, protecting from induction of inflammation[35, 68].

By studying the impact of commensals and their derived metabolites, a better understanding of the host-immune-microbiome relationship can be attained and manipulated for the treatment of disease.

Chapter 2: Purification of Capsular Polysaccharide Complex from Gram Negative

*Work featured in this chapter was published in *Bacterial Polysaccharides: Methods and Protocols* (Alvarez, C. A. and Cobb, B. A. , 2019, pp 25-35 (ref # 122))

2.1 Abstract

Capsular polysaccharides are a dominant class of antigens from bacteria, both pathogenic and symbiotic or commensal. With the rise of awareness for the influence of the microbiota over immune system development and immune homeostasis, analysis of the antigens is more important than ever. Here we describe a method for the isolation of capsular polysaccharide from gram negative bacteria, with the purification of polysaccharide from the commensal bacterium *Bacteroides fragilis* serving as an example. The method efficiently removes all detectable endotoxin and other lipid components, proteins, and nucleic acids, providing a source of capsular polysaccharide for immunologic study.

2.2 Introduction

A wide range of microorganisms, each occupying a specific niche and role, populates the human body and is collectively known as the microbiome. Over the last couple of decades, it has become clear that the composition of the microbiome plays a critical role in the maintenance of homeostasis. The mechanisms underlying this homeostatic function are quite diverse, ranging from nutrient metabolism and niche competition to immunologic development [69-72]. From an immune perspective, the microbiota produces many immunogens and antigens that have been shown to drive immune system development and bias the host against deleterious inflammatory responses common to autoimmune

and allergic diseases [67, 73-76]. These include proteins, lipoproteins, nucleic acids, endotoxin (lipopolysaccharide; LPS) and capsular polysaccharides.

Capsular polysaccharides represent the outermost surface of encapsulated bacteria, such as *Bacteroides fragilis*, making these molecules the first point of contact with the immune system. Of the eight different capsular polysaccharides found on *B. fragilis* [77], polysaccharide A (PSA) and B (PSB) are zwitterionic, possessing both positive and negative charges in their repeating units [78]. This property has been shown to enable their ability to activate CD4⁺ T cells through major histocompatibility complex class II-mediated presentation [34, 79], which leads to immune inhibition and resistance to inflammatory disease [67, 73].

However, it is critical to separate the capsular polysaccharide from underlying LPS, protein and nucleic acid for immunologic evaluation and study.

Here, we describe the purification of capsular polysaccharide from gram negative bacteria, which is based on previously reported methods [78, 80] and our experience with *B. fragilis* and PSA [34, 81, 82]. The procedure begins with a hot phenol extraction, which breaks down the bacteria and leads to the precipitation of nucleic acids and proteins, leaving the lipid and carbohydrate fractions in the aqueous phase. Residual phenol is removed from the aqueous phase by ethyl ether extraction followed by evaporation of residual ethyl ether using a rotary evaporator. The extracted lipids/LPS and polysaccharides are then treated with DNase, RNase, and proteinase K to digest any remaining traces of nucleic acids and proteins respectively. The resulting LPS and capsular polysaccharide mixture is separated by size exclusion chromatography in deoxycholate, which

disaggregates the LPS so that it runs as a relatively small molecule compared to the very large (>300 kDa) polysaccharides. LPS-free polysaccharide is pooled and deoxycholate removed through dialysis to yield between 100 and 400 mg of polysaccharide from 20 L of log-phase liquid culture.

2.3 Materials

In this method, the bacterial growth step is skipped, since culture conditions can vary wildly, depending on the bacterial species/strain. The extraction is suitable for any capsular polysaccharide from a gram-negative bacterium. Thus, the starting material for this purification is pelleted bacteria from 20 L of log-phase growth culture. The large scale is due to the relative expense and time required for the preparation, making repeated preparations needlessly inefficient.

Moreover, all solutions are made with ultrapure (18 M Ω /cm) water, and hazardous waste disposal is done according to the appropriate local regulations.

2.3.1 Solutions, Reagents and Supplies

1. 1.0 M Tris, pH 7.5: 1.0 M solutions of both Tris-HCl (157.60 g in 1 L water; do not adjust pH) and Tris-base (121.14 g in 1 L water, do not adjust pH). Titrate 500 mL Tris-base with Tris-HCl in a 1 L beaker with stirring until the pH reaches 7.5. Filter sterilize and store at room temperature.
2. 1.0 M MgCl₂: Dissolve 95.21 g MgCl₂ in 1 L of water. Filter sterilize and store at room temperature.

3. 1.0 M CaCl₂: Dissolve 110.98 g CaCl₂ in 1 L of water. Filter sterilize and store at room temperature.
4. 1.0 M EDTA, pH 8.0: Dissolve 146.12 g anhydrous ethylenediaminetetraacetic acid (EDTA) in 250 mL water. Adjust pH to 8.0 with NaOH under constant stirring. The EDTA will not completely go into solution until near neutral pH is reached. Dilute to 500 mL, filter sterilize and store at room temperature.
5. 5 L sterile water stored at room temperature.
6. 2 M NaCl: Dissolve 116.8 g NaCl in 1 L of water. Filter sterilize and store at room temperature.
7. Approximately 4 L of 95% ethanol: Store at room temperature until indicated otherwise.
8. Phosphate buffered saline (PBS): Dissolve 8 g NaCl (137 mM), 0.2 g KCl (2.7 mM), 1.44 g Na₂HPO₄ (10 mM), and 0.24 g KH₂PO₄ (1.8 mM) in 800 mL water. Adjust pH to 7.4 with HCl. Bring to 1 L with water, filter sterilize and store at room temperature.
9. 2 L Ethyl ether. Store at room temperature.
10. Glacial acetic acid. Store at room temperature.
11. 500 g phenol (see **Note 1**). Store at room temperature.
12. 1.0 g Pronase (Millipore Sigma Catalog #53702). Store at -20 °C.
13. 500 mg Ribonuclease A (Worthington Biochemical Corp. Catalog # LS005650). Store at -20 °C.

14. 100 mg Deoxyribonuclease Type I (Worthington Biochemical Corp. Catalog # LS002007). Store at -20 °C.
15. Column running buffer: Dissolve 60 g deoxycholic acid, ultrapure grade (30 g/L), 7.5 g glycine (50 mM), and 7.44 g EDTA (10 mM) into 1.5 L water (see **Note 2**). Adjust pH to 9.8 with NaOH. Bring to 2 L with water. Do not filter and store at room temperature.
16. Pro-Q Emerald 300 lipopolysaccharide Gel Stain Kit (ThermoFisher). Store components as instructed by the manufacturer.
17. Sephacryl S-400 column (100 cm x 5 cm) fitted to a peristaltic pump and fraction collector.
18. Dialysis membrane tubing (3 in. diameter; 12-14 kDa MWCO) (see **Note 3**).
19. Glass pipettes (25 mL).

2.3.2 Special Equipment

1. Heavy-duty stir plate.
2. Glass beads (~5 mm diameter).
3. Six 250 mL phenol/chemical resistant centrifuge bottles with gaskets.
4. Stand mixer.
5. Separatory funnel (2 L) with large ring stand.
6. Rotary evaporator with 1 L sample flask.
7. Lyophilizer.
8. Peristaltic pump and fraction collector

2.4 Methods

2.4.1 Harvest and Phenol Extraction

1. Setup extraction equipment in a fume hood, including a water bath pre-warmed to 68 °C and a stand mixer (Fig. 1).
2. Warm 1 L of water and the 500 g bottle of solid phenol to 68 °C in the water bath until all of the phenol is melted.
3. Once up to temperature, add 167 ml of pre-warmed water to the phenol to make it 75 %.
4. Resuspend the frozen bacterial pellet in 667 ml of 68 °C water, making sure that no chunks of bacterial pellet remain.
5. Transfer the resuspended bacteria into a 4 L glass beaker, and place into the 68 °C water bath.
6. Add about 250 mL equivalent volume of glass beads to the sample.
7. Place the mixer blades into the sample so that the blades are just above the bottom of the beaker (Fig. 1), and turn on at a speed fast enough that the glass beads are well agitated.
8. Add all of the 75 % pre-warmed phenol to the sample mixture and allow robust mixing for 30 minutes (see **Note 4**).
9. Remove the stand mixer and add a large stir bar to the sample, cover with several layers of Parafilm and aluminum foil, and stir overnight on a heavy duty stir plate at 4 °C. Be sure to use secondary containment.

10. Using the chemically-resistant 250 mL centrifuge bottles, centrifuge the sample at 10,000 x g for 20 minutes at 4 °C.
11. Very carefully (see **Note 5**) decant the top aqueous layer using a glass pipet, placing the extract into a clean 1 L glass bottle.
12. Repeat the centrifugation until the entire sample has been centrifuged, combining the top aqueous phase in the 1 L glass bottle, and the waste in the waste vessel.

2.4.2 Ether Extraction

1. Prepare a 2 L separatory funnel by applying stopcock grease to the fittings.
2. Add approximately 400 ml of sample and an equal volume of ethyl ether to remove dissolved phenol.
3. Close the funnel and shake vigorously for 5 minutes (CAUTION, see **Note 6**).
4. Allow the mix to separate into two layers (top, ethyl ether; bottom, aqueous) for about 20 minutes by placing the funnel on a ring stand.
5. Slowly allow the bottom aqueous phase, which contains the lipids and carbohydrates, out of the funnel into a clean 1 L glass bottle (see **Note 7**). Discard the top layer into an appropriate waste vessel for ethyl ether disposal.
6. Repeat until the entire phenol extract has been extracted with ethyl ether, combining the bottom phase into one or more 1 L glass bottles.

7. Repeat the ethyl ether extraction on the entire sample once more.
8. Setup a rotary evaporator in a fume hood, circulating cool water through the condenser and pre-warming the water bath to 60 °C.
9. Place approximately 500 mL of the ether-extracted sample into the sample flask, and evaporate the residual ethyl ether and concentrate the sample for approximately 1 hour, being careful to guard against boiling bumps in the first 10 minutes.
10. Remove the sample, saving it in a fresh 1 L glass bottle.
11. Repeat the evaporation until all of the sample is complete, combining the final product together.
12. Place the sample in pre-hydrated dialysis tubing (see **Note 3**), and dialyze against water supplemented with 0.05% sodium azide at 4 °C (see **Note 8**).

2.4.3 Digestion and Precipitation

1. Remove the sample from dialysis using aseptic technique into sterile 1 L bottle(s).
2. Measure the approximate volume of the sample and calculate 6.5 % of this value.
3. In a 50 mL conical tube, add calculated volume of 1.0 M Tris, pH 7.5.
4. Add 1.0 M MgCl₂ and 1.0 M CaCl₂ to make the Tris solution contain 20 mM each.

5. Add RNase A and DNase Type I to the Tris solution such that the final concentration in the sample will be 0.33 mg/mL and 0.07 mg/mL respectively (see **Note 9**).
6. Filter sterilize the enzyme mixture, then add to the sample.
7. Cover/close the bottle and incubate overnight at 37 °C.
8. Re-adjust the pH of the sample to 7.5 with 1.0 M NaOH if necessary (see **Note 10**).
9. Weigh enough Proteinase K to achieve a final concentration of 0.33 mg/mL, dissolve it in 5 mL 1.0 M Tris, pH 7.5, filter sterilize the enzyme solution, and add it to the sample.
10. Incubate overnight at 37 °C.
11. Place several liters of 95 % ethanol in the -20 °C freezer overnight.
12. Repeat the Proteinase K digest with fresh enzyme prepared as before.
13. Incubate 2 hours 37 °C.
14. Add enough 1.0 M EDTA, pH 8.0 to the sample to make the final concentration 50 mM EDTA.
15. Add a sterile stir bar and stir for 30 minutes at 4 °C.
16. Add 11 % of the sample volume of 2 M NaCl (200 mM final concentration).
17. Precipitate the LPS and capsular polysaccharide by dividing the sample into 200 mL aliquots in as many 1 L glass bottles as necessary. Add 800 mL ice cold (-20 °C) ethanol, close and mix well (see **Note 11**).
18. Incubate overnight at -20 °C.

19. Collect precipitate by centrifugation of the samples at 10,000 x g at 4 °C for 1 hour (see **Note 12**). It is okay to use the same centrifuge bottles over and over, stacking the sample in the pellet.
20. Decant the ethanol/water and dry the pellets by inversion for 2 hours.
21. Resuspend all of the pellets in a total of no more than 30 mL Column Running Buffer (see **Note 13**).

2.4.4 Chromatography

1. Wash the S-400 column with 600 mL of 0.1 M NaOH at 1.5 mL/min.
2. Equilibrate the column with 2 L Column Running Buffer at 1.5 mL/min.
3. Load the equilibrated column with no more than 30 mL of sample. If the sample is in greater volume, separate the sample into multiple column runs.
4. Run the column with 2 L Column Running Buffer, collecting 20 mL fractions between 500 mL and 1500 mL elution volume.
5. Regenerate the column by repeating the 600 mL 0.1 M NaOH wash and re-equilibration in steps 1 and 2 before running another sample to prevent LPS contamination.

2.4.5 Fraction Analysis and Sample Pooling

1. Using standard SDS-PAGE techniques and sample loading buffer, run 15 µL of each fraction on a 10 % continuous polyacrylamide gel (see **Note 14**) until the blue loading dye has just exited the bottom of the gel.

2. Stain the gel using the Pro-Q Emerald 300 lipopolysaccharide Gel Stain Kit according to the manufacturer's protocol. This kit actually stains carbohydrates and will detect both LPS and capsular polysaccharide with very high sensitivity (Fig. 2).
3. Pool clean capsular polysaccharide fractions that lack detectable LPS.
4. Place the entire sample into dialysis against continuous running water (see **Note 15**) for at least 1 week to remove the deoxycholate.
5. Collect and freeze dry the final sample using a lyophilizer.
6. Collect and measure the dry weight on an analytical balance.

2.4.6 Quality Check

1. Make a 1 mg/mL solution of capsular polysaccharide in water.
2. Perform a wavelength absorbance scan between 200 and 350 nm in a 1 cm path length cuvette. The absorbance at 260 and 280 nm should be less than 0.1.
3. Run 20 µg of sample on SDS-PAGE as before, staining with Pro-Q. No detectable LPS should be visible.
4. For PSA from *Bacteroides fragilis*, ¹H NMR is performed for the known spectrum and a lack of non-PSA resonant peaks.

2.4.7 Storage

1. Dissolve the entire sample in water.
2. Make 1 and 5 mg aliquots in small glass vials and freeze dry.

3. Seal the tubes and store the dried polysaccharide at -80 °C.

2.5 Notes

1. Phenol should be purchased as a single bottle of 500 g of solid phenol. The entire 500 g will be used in liquid phase, thus eliminating the need to measure the solid and increasing safety. Upon use, the glass bottle the phenol is supplied in can become the waste container for hazardous waste disposal.
2. Use caution when making this buffer. Begin by dissolving the glycine and EDTA. Then add the deoxycholate. Powdered deoxycholate is very light and will disperse into the air with the slightest agitation. As a result, use slow and careful movements when weighing and dispensing the deoxycholate to minimize this effect. Use goggles and a respirator, as the dispersed deoxycholate is very irritating to mucous membranes. Use of a fume hood is incompatible with this procedure due to the air flow. Finally, deoxycholate will not dissolve in water until the pH is at least 8.5. Thus, NaOH must be added with constant mixing and pH monitoring as the deoxycholate is added. It can take 30 minutes or more for all deoxycholate to enter solution. Adjust the pH to 9.8 with NaOH, then bring the final volume to 2 L with water.
3. In order to prepare the dialysis tubing, cut the desired length, allowing for at least 50 % sample swelling, boil in 5 mM EDTA, pH 8.0 for 10 minutes, rinse twice with room temperature water and store at 4°C in 20 % ethanol until use. Do not allow the membrane to dry out once re-hydrated.

4. Addition of 75 % phenol to the resuspended bacteria will cause an immediate lysis of the bacteria. The resulting solution will have a viscous chocolate milk appearance.
5. If things are going well, after the spin you should see a large viscous and sticky tan-colored pellet and a relatively small amount of a tan/greenish-colored liquid on the top, which is the desired fraction. The pellet is very loose, thus caution is required in removing the top layer. In addition, it is better to get some of the pellet in the sample to get all the top aqueous phase, but if this happens, a repeat spin in clean bottles will be necessary to remove the bottom layer. Finally, the bottom layer is mostly phenol and must be discarded appropriately.
6. It is critically important to vent the separatory funnel often. Gas is released upon the first several shakes, and will build up in the funnel. This could lead to glass failure if not vented. Use a face shield in addition to goggles and other standard chemical and laboratory safety personal protective gear.
7. It is best to get all of the bottom phase in the first extraction, even if some of the top phase is collected. Upon the second ethyl ether extraction, the separation will be clearer and easier to prevent top layer contamination.
8. The sample is large at this point, thus splitting the sample into two parts is often easiest. Dialysis should have a sample: water ratio of at least 1:10, changing the water 6 times after at least 4 hours has passed with stirring each time.

9. The amount of RNase A and DNase Type I is based on the sample volume, not the 1.0 M Tris volume calculated in step 2, section 3.3.
10. Use a sterile pipet tip and drop sample onto pH paper to estimate the pH. Do not contaminate the sample by using a pH probe.
11. The ethanol must be very cold for optimal precipitation. The sample will become milky white immediately upon addition of the ethanol.
12. This will take more than 1 spin to collect the large volume of sample. It is okay to use the same centrifuge bottles over and over, stacking the sample in the pellet. Also, much of the precipitate will stick to the walls of the original 1 L glass bottles. This is normal and desirable. Once all liquid has been removed for centrifugation, dry the stuck precipitate by inverting the bottles on paper towels for at least 2 hours.
13. The Column Running Buffer contains a high concentration of detergent, and is therefore soapy. Avoid making bubbles. Also, all pellets and glass bottle precipitates should be combined into a single 30 mL sample. The final sample will have a brown tone, but should be free of visible particulates.
14. The SDS-PAGE gel does not need a stacking gel, and the samples do not need to be boiled before loading. The LPS will run just above the dye front, while the capsular polysaccharide will run high, just inside the wells at the top (Fig. 2).
15. A large plastic bucket from a hardware store, cleaned to laboratory standards, can be used for this purpose, making sure there are no sharp edges or imperfections before use. Place the bucket in a sink, fill with dH₂O, add the

sample in a dialysis bag, and allow the water to continuously flow, slowly. Do this at 4 °C.

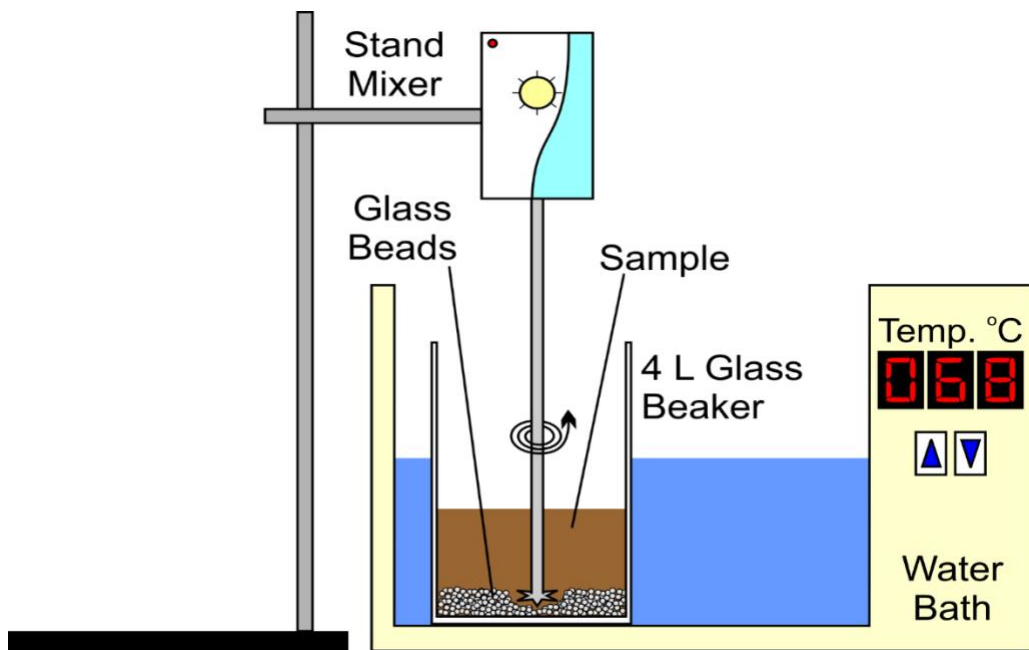


Fig. 1 Phenol extraction assembly for the initial extraction of LPS and capsular polysaccharide from intact gram negative bacteria. Resuspended bacteria are combined with 75 % phenol in a 4 L beaker at 68 °C in a water bath. Glass beads are placed in the beaker and agitated with a stand mixer. The extraction should be performed within a fume hood.

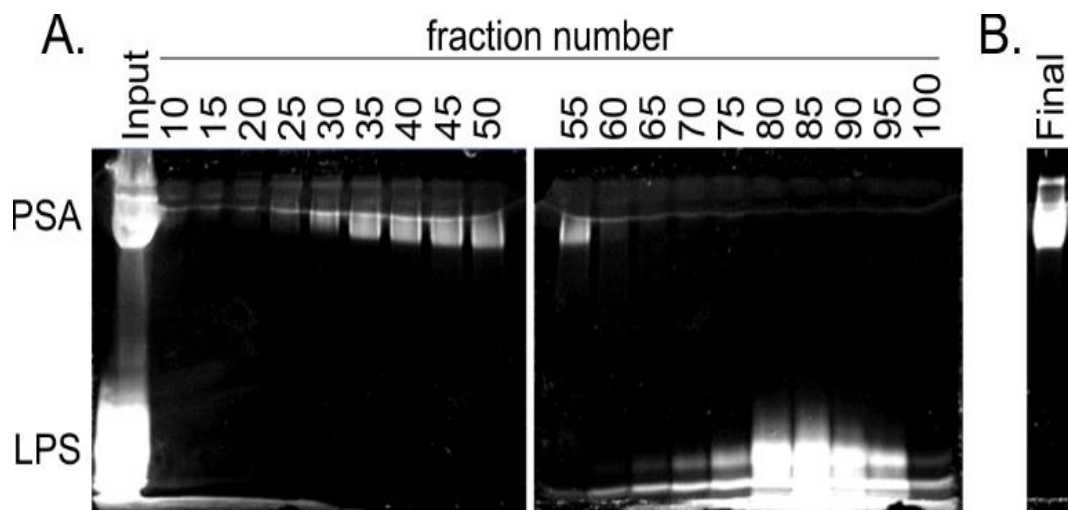


Fig. 2 Pro-Q Emerald stained SDS-PAGE gels from the purification of PSA from *B. fragilis*. (A) In the first lane, 2 μ L of the sample loaded onto the column was run as the input control. All other lanes contain 20 μ L of the fraction indicated, with each collected fraction being 20 mL. “Clean” PSA was pooled from fractions 30 to 50, giving a final PSA sample volume of 420 mL containing approximately 300 mg of PSA. (B) The final PSA sample after pooling and dialysis, showing the lack of detectable LPS.

**Chapter 3: CD45Rb-Low Effector T cells Require IL-4 to Induce IL-10 in
FoxP3 Tregs and to Protect Mice from Inflammation**

*Work featured in this chapter was published in PLOS One(Jones, M. B.,
Alvarez, C. A., Johnson, J. L., Zhou, J. Y., Morris, N., & Cobb, B. A. , 2019,
14(5), e0216893 (ref # 118))

3.1 Abstract

CD4⁺ effector/memory T cells (Tem) represent a leading edge of the adaptive immune system responsible for protecting the body from infection, cancer, and other damaging processes. However, a subset of Tem cells with low expression of CD45Rb (Rb^{Lo}Tem) has been shown to suppress inflammation despite their effector surface phenotype and the lack of FoxP3 expression, the canonical transcription factor found in most regulatory T cells. In this report, we show that Rb^{Lo}Tem cells can suppress inflammation by influencing Treg behavior. Co-culturing activated Rb^{Lo}Tem and Tregs induced high expression of IL-10 *in vitro*, and conditioned media from Rb^{Lo}Tem cells induced IL-10 expression in FoxP3⁺ Tregs *in vitro* and *in vivo*, indicating that Rb^{Lo}Tem cells communicate with Tregs in a cell-contact independent fashion. Transcriptomic and multi-analyte Luminex data identified both IL-2 and IL-4 as potential mediators of Rb^{Lo}Tem-Treg communication, and antibody-mediated neutralization of either IL-4 or CD124 (IL-4R α) prevented IL-10 induction in Tregs. Moreover, isolated Tregs cultured with recombinant IL-2 and IL-4 strongly induced IL-10 production. Using house dust mite (HDM)-induced airway inflammation as a model, we confirmed that the *in vivo* suppressive activity of Rb^{Lo}Tem cells was lost in IL-4-ablated Rb^{Lo}Tem cells. These data support a model in which Rb^{Lo}Tem cells communicate with Tregs using a combination of IL-2 and IL-4 to induce robust expression of IL-10 and suppression of inflammation.

*Work featured in this chapter was published in PLOS One(Jones, M. B., Alvarez, C. A., Johnson, J. L., Zhou, J. Y., Morris, N., & Cobb, B. A. , 2019, 14(5), e0216893 (ref # 118))

3.2 Introduction

Regulatory T cells (Tregs) are critical for the maintenance of immune homeostasis. The most widely recognized and studied subset of Tregs express the transcription factor FoxP3 and can be induced peripherally or develop directly in the thymus [83-85]; however, FoxP3⁻ type 1 regulatory cells (Tr1) are also well-characterized [86, 87]. Another CD4⁺ T cell subset known to have regulatory/suppressive properties are those lacking FoxP3 while expressing low concentrations of the activation marker CD45Rb (Rb^{L0}) at the cell surface. These Rb^{L0} T cells inhibit the induction of wasting disease in SCID mice [88], type 1 diabetes [89], a plant antigen-based model of asthma [90], and the formation of adhesions [91]. In agreement with these reports, we recently found that the polysaccharide antigen PSA from *Bacteroides fragilis* significantly decreased susceptibility to the development of pulmonary inflammation through activation and expansion of CD4⁺FoxP3⁻CD45Rb^{L0} effector-memory (CD62L⁻CD44⁺) T cells (Rb^{L0}Tem)[67, 68, 92].

Rb^{L0}Tem cells are known to depend upon IL-10 for their protective efficacy [93, 94]. Consistent with this, we found that the suppressive activity of Rb^{L0}Tem cells required IL-10 in both humans *in vitro* [95] and mice *in vivo* [67, 68]. In an *in vivo* model in which all cells lacked IL-10, the Rb^{L0}Tem cells failed to protect the

animals from pulmonary inflammation [67]. However, reciprocal adoptive transfer experiments in which activated wild type (WT) or IL-10-deficient (IL-10^{-/-}) Rb^{Lo}Tem cells were given to WT or IL-10^{-/-} recipients, we discovered that IL-10 was dispensable in the Rb^{Lo}Tem cells but not in the recipient [68]. Moreover, adoptive transfer of IL-10^{-/-} Rb^{Lo}Tem cells induced IL-10 expression in CD4⁺FoxP3⁺ Tregs in the lung [68], suggesting a model in which Rb^{Lo}Tem cells suppress inflammation by the selective induction of IL-10 in FoxP3⁺ Tregs *in vivo* through an unknown mechanism.

In this study, we report the discovery of a mechanism by which Rb^{Lo}Tem cells communicate with and drive suppressive activity of FoxP3⁺ Tregs to regulate inflammation. Consistent with our *in vivo* studies [68], co-cultured Rb^{Lo}Tem cells induced FoxP3⁺ Tregs to secrete high concentrations of IL-10 *in vitro*.

Conditioned media from activated Rb^{Lo}Tem cells also induced IL-10 in FoxP3⁺ Tregs both *in vivo* and *in vitro*, demonstrating cell-contact independence in the communication pathway between these cells. Deep sequencing transcriptomics of activated Rb^{Lo}Tem cells versus CD45Rb^{Hi} T naïve cells identified potential soluble mediators, and antibody-mediated neutralization experiments suggested that both IL-2 and IL-4 were necessary for IL-10 induction in Tregs.

Supplementation of Treg media with recombinant IL-2 and IL-4 confirmed this *in vitro*, while the use of IL-4-deficient Rb^{Lo}Tem cells showed a lack of protective efficacy in a model of pulmonary inflammation when compared to WT cells.

These results reveal an intrinsic IL-2 and IL-4-dependent T cell crosstalk network connecting the suppressive capacity of Rb^{Lo}Tem cells with canonical FoxP3⁺

Tregs, which could potentially be harnessed for the treatment of inflammation-mediated diseases.

3.3 Methods

3.3.1 Mice.

C57BL/6 (Stock #000664), IL-10-eGFP (B6.129S6-Il10^{tm1Flv}/J, Stock #008379), IL-10-null (B6.129P2-Il10^{tm1Cgn}/J, Stock #002251), FoxP3-RFP (C57BL/6-FoxP3^{tm1Flv}/J), and IL-4-knockout (B6.129P2-Il4^{tm1Cgn}/J) mice, all on the C57BL/6 background, were purchased from the Jackson Laboratory (Bar Harbor, ME). FoxP3-eGFP animals were a kind gift of Drs. Rudensky and Letterio. Mice were fed standard chow (Purina 5010) on a 12-hour light/dark cycle in a specific pathogen free facility. Enrichment and privacy provided in mating cages by 'love shacks' (Bio Serv 53352-400). Mouse studies, and all animal housing at Case Western Reserve University were approved by and performed according to the guidelines established by the Institutional Animal Care and Use Committee of CWRU.

3.3.2 Primary splenic T cells.

Primary splenocytes were isolated from freshly harvested spleens, and reduced to a single cell suspension by passing them through a sterile 100µM nylon mesh cell strainer (Fisher Scientific, Hampton, NH). For splenic T cell enrichment,

single cell suspensions were labeled with anti-mouse CD4 magnetic microbeads, or alternatively negatively selected to yield untouched CD4 cells, and positively selected for CD25 by a mouse regulatory T cell isolation kit (Miltenyi Biotec, San Diego, CA), and separated with an AutoMACS Pro Separator (Miltenyi Biotec, San Diego, CA), per manufacturer's instructions.

3.3.3 Pulmonary inflammation and adoptive transfer.

HDM Model: Mice were challenged with house dust mite antigen (HDM, *D. Farinae*, GREER, Lenoir, NC) by intranasal delivery of 20µg HDM/dose in PBS on days 0-4 and 7-11 and sacrificed on day 14 [96]. For adoptive transfer, 60,000 Rb^{Lo}Tem cells were harvested by FACS from FoxP3-eGFP reporter mice and i.v. injected on day 6. Animals were anesthetized with 3% isoflurane (Baxter) with an anesthesia system (VetEquip, Livermore, CA) for intranasal administration. Euthanasia, BALf recovery, and lung tissue preparation was performed as previously reported [67, 68]. BALf automated differentials were acquired by a HemaVet 950 Hematology Analyzer.

3.3.4 Flow cytometry and cell sorting.

For splenic T cell sorting, magnetic bead-mediated positively selected CD4⁺ cells were stained with combinations of antibodies (0.5µg/mL per) to CD62L-PE (BioLegend, San Diego, CA) or CD62L-BB515 (BD Bioscience), CD44-APC (BioLegend, San Diego, CA), CD45Rb-APC/Cy7 (BioLegend, San Diego, CA), CD124 (1µg/mL, BD Biosciences, San Jose, CA), and CD25-BV421 (BD

Biosciences, San Jose, CA). For Tregs, FoxP3-RFP reporter signal was used for FACS. Cells were washed twice in MACS buffer (Miltenyi Biotec, San Diego, CA) before sterile cell sorting using a FACSAria (BD Biosciences, San Jose, CA) with the support of the Cytometry & Imaging Microscopy Core Facility of the Case Comprehensive Cancer Center. Analysis of all FACS data was performed using FlowJo v10 (Tree Star, Inc., Ashland, OR).

3.3.5 Cell culture.

After flow sorting, cells were cultured in 96-well plates (Corning, Corning, NY) at 50,000 cells per type per well in advanced RPMI (Gibco/Fisher Scientific, Waltham, MA) supplemented with 5% Australian-produced heat-inactivated fetal bovine serum, 55 μ M β -mercaptoethanol, 100U/mL and 100 μ g/mL Penicillin/Streptomycin, and 0.2mM L-glutamine (Gibco/Fisher Scientific, Waltham, MA) at 5% CO₂, 37°C. For activating conditions, wells were coated with α CD3 ϵ (eBioscience, San Diego, CA) at 2.5 μ g/mL in PBS then incubated at 37°C for 4 hours followed by two washes with PBS before receiving cells. For fixation studies, indicated cell types were resuspended in 2% paraformaldehyde in PBS for 10 minutes on ice. Cells were washed twice in PBS before being co-cultured with live CD4⁺FoxP3⁺ cells. All co-culture experiments were performed at 1:1 cell ratio, except for the experiments in Fig 3C, which were performed by maintaining constant Tconv cell numbers (50k) and altering the number of Tregs relative to the 50k Tconv, as indicated.

3.3.6 ELISA, blocking, supplementation and Luminex.

Cytokine levels were analyzed by standard sandwich ELISA performed as per manufacturer's instructions (BioLegend, San Diego, CA), modified to utilize europium-conjugated streptavidin (Perkin-Elmer), and detected with a Victor V3 plate reader (Perkin Elmer, San Jose, CA). Blocking experiments utilized antibodies to IFN γ (10 μ g/mL, BioLegend, San Diego, CA), IL-21 (10 μ g/mL, eBioscience, San Diego, CA), IL-22 (10 μ g/mL, eBioscience), CSF2 (10 μ g/mL, eBioscience), IL-9 (1 μ g/mL, eBioscience), IL-13 (2 μ g/mL, eBioscience), IL-4 (1 μ g/mL, eBioscience), IL-24 (2 μ g/mL, eBioscience), IL-3 (1 μ g/mL, eBioscience), Neuropilin-1 (1 μ g/mL, R&D Systems, Minneapolis, MN), CD124 (1 μ g/mL, BD Biosciences, San Jose, CA), and corresponding isotype controls IgG1 and IgG2a (BioLegend, San Diego, CA). For CD124 blocking experiments, indicated cell types were incubated with 1 μ g/mL α CD124 at 4°C for 15 minutes, washed twice with PBS, then combined into co-culture. Supplementation assays were performed with recombinant mouse IL-2 and IL-4 (R&D Systems, Minneapolis, MN) at the indicated concentrations. For Luminex assays, media from indicated cultured populations were snap frozen in liquid nitrogen and sent to Eve Technologies (Calgary, Ontario, Canada) for mouse 32-plex and TGF- β 3-plex analysis.

3.3.7 RNAseq and analysis.

For RNA quantitation, CD4⁺FoxP3⁺ (Treg), CD4⁺FoxP3⁻CD45Rb^{Hi}CD62^{Hi}CD44^{Lo} (Rb^{Hi}Tn), CD4⁺FoxP3⁻CD45Rb^{Lo}CD62^{Lo}CD44^{Hi} (Rb^{Lo}Tem) cells were flow

sorted as above, pelleted and snap frozen in liquid nitrogen. RNA extraction and RNAseq was performed at Ambry Genetics. Initial processing of the data was performed by using the trimmomatic [97] program to trim the poor-quality reads, and fastQC to investigate read quality. TopHat [98] was used to align the reads to the “mm10” genome guided by the Gencode vm4 [99] annotations. To count the number of reads aligning to each feature in Gencode vm4, we used htseq-count [100]. RPKM values were calculated in R, and the differential expression analysis between “Hi” and “Lo” samples was performed using the negative binomial test implemented in DEseq2 [101].

3.3.8 Histology and microscopy.

Tissues were blocked, sectioned, and stained with H&E by the Case Western Reserve University Tissue Procurement and Histology Core Facility, and at AML Laboratories, Inc. (Jacksonville, FL). Unstained sections were stained with rat-anti-EpCAM-AF488 (eBioscience, San Diego, CA) or rat-anti-EpCAM-AF594 (BioLegend, San Diego, CA) at 6µg/mL, and rabbit-anti-myeloperoxidase (1:100, Abcam, Cambridge, MA) then either anti-rabbit-APC (Thermo/Fisher, Waltham, MA) or anti-rabbit-AF488 (Jackson ImmunoResearch, West Grove, PA) at 1:1000. Confocal analysis and imaging were performed on a Leica SP5 confocal microscope; H&E images were acquired with a Leica DM IL LED.

3.3.9 Clinical Scoring.

Scoring of H&E-stained lung tissues was performed by Dr. Cobb in a blinded fashion based on the rubric shown in Table 1, with a maximum score of 9 characterized by severe airway epithelial hyperplasia and large numbers of infiltrating cells disseminated throughout the tissue. H&E stained lung sections were scored for epithelial cell hyperplasia, infiltration of immune cells, and localization of immune cells on a zero to 3 scale for each parameter. Final clinical scores were the sum of each parameter for each tissue.

3.3.10 Data analyses.

All data are represented by mean \pm SEM from at least 3 independent experiments, with the exception of the RNAseq, which was performed in duplicate for each subset. Pulmonary inflammation data sets include a minimum of four, but more commonly six animals per group per experiment. Data and statistical measurements were generated with GraphPad Prism (v5.0). For comparisons between two groups, Student's *t*-test was used; comparisons between multiple groups utilized analysis of variance.

3.3.11 Data availability.

Raw and processed data files for all RNA deep sequencing have been deposited in the NCBI Gene Expression Omnibus under accession number GSE89241.

3.4 Results

3.4.1 *Rb^{Lo}* Tem cells induce IL-10 in FoxP3⁺ Tregs

Our previous studies revealed that conventional CD4⁺ T cells activated by the polysaccharide PSA from the capsule of *Bacteroides fragilis* can influence FoxP3⁺ Tregs to produce IL-10 through an unknown pathway [67, 68]. Here, we investigated the ability of CD4⁺ T cells to influence Tregs and their production of IL-10 in the absence of PSA. CD4⁺CD25⁺ Tregs and CD4⁺CD25⁻ Tconv cells were isolated from WT mice using either magnetic beads (M) or sterile flow sorting (FI), and stimulated with anti-CD3 ϵ antibody alone or in co-culture for different amounts of time. Despite having not been previously exposed to PSA, we found that when cultured together, Tregs and Tconv cells synergistically produced IL-10 at 72 hours, while IFN γ production was simply additive (Figs 3A-B). Moreover, variations of the ratio of Treg:Tconv demonstrates that the amount of IL-10 is proportional to the number of Tregs, not the number of Tconv cells (Fig 3C).

PSA exposure expands a CD4⁺FoxP3⁻CD45Rb^{Lo} T cell population in both humans [95] and mice [67, 92], and this population was found to induce IL-10 production by lung-localized FoxP3⁺ Tregs [68]. We therefore isolated CD4⁺FoxP3⁻CD45Rb^{Lo} (FoxP3⁻Rb^{Lo}), CD4⁺FoxP3⁻CD45Rb^{Hi} (FoxP3⁻Rb^{Hi}), and CD4⁺FoxP3⁺ Tregs (FoxP3⁺) from PSA-naïve FoxP3-eGFP reporter mice and stimulated them as before with anti-CD3 ϵ . We found that while the FoxP3⁻Rb^{Lo} subset produced some IL-10 alone, the IL-10 concentration was increased over 2-fold in co-culture with FoxP3⁺ cells on day 3 (Fig 3D). IFN γ trended down but was not significant while IL-2 was significantly reduced in co-culture (Fig 3D).

Importantly, the FoxP3⁻Rb^{Hi} population, despite their ability to produce IL-2, did not induce significant IL-10 secretion *in vitro*.

To further clarify the identification of T cells responsible for communicating with FoxP3⁺ Tregs, CD4⁺FoxP3⁺ Tregs with or without CD25, CD4⁺ naïve (Tn; CD62L⁺CD44⁻), effector memory (Tem; CD62L⁻CD44⁺) and central memory (Tcm; CD62L⁺CD44⁺) T cells from FoxP3-eGFP mice were isolated and stimulated as before in various combinations. Tem cells were the only subset to produce IL-10 alone, and the only ones to synergistically induce IL-10 in co-culture with Tregs (Figs 3E-F), suggesting that the T cell subset responsible for the Treg IL-10 effect is antigen experienced and are most likely CD4⁺FoxP3⁻CD62L⁻CD44⁺CD45Rb^{Lo} (Rb^{Lo}Tem) cells. The presence (Fig 3E) or absence (Fig 3F) of the IL-2R α (CD25) on the Treg population (see Fig 10 for the gating strategy) did not have an impact on the synergistic interaction between these cells. Finally, we isolated Rb^{Lo}Tem and CD4⁺FoxP3⁻CD62L⁺CD44⁻CD45Rb^{Hi} (Rb^{Hi}Tn) T cells (see Fig 11 for the gating strategy) and compared their ability to induce IL-10 synergy with FoxP3⁺ Tregs. Only the Rb^{Lo}Tem cells produced IL-10 alone and synergistically with FoxP3⁺ Tregs (Fig 3G). These findings align the identity of the cells capable of stimulating IL-10 production in Tregs with those which are selectively expanded by PSA [67, 68, 92]. More importantly, the data demonstrate that Rb^{Lo}Tem cell communication with Tregs is independent of PSA, and is therefore an intrinsic property of this regulatory T cell subset.

3.4.2 IL-10 synergy is unique among common cytokines

Although IL-10 is necessary for Rb^{L0}Tem cell-mediated immune suppression [67, 68], we performed multiplex Luminex analysis in order to identify other important cytokines and chemokines. We found that IL-10 was the only cytokine tested that displayed synergistic increases when Rb^{L0}Tem and FoxP3⁺ Tregs were in co-culture (Fig 4A). Two other cytokines closely aligned with immune regulation, TGF- β 1 and TGF- β 2, were significantly down-regulated in co-culture compared to the combined production of each cell population in isolation (Fig 4A). All other cytokines and chemokines fell into two categories – reduced in co-culture (Fig 4B) or unchanged in co-culture (Fig 4C). Notable molecules with robust decreases included IL-5, IL-6, IL-13, TNF α , and GM-CSF (Fig 4B), while a notable unchanged molecule was IL-4 (Fig 4C).

3.4.3 IL-10 synergy depends on a soluble mediator

Our data suggested that Rb^{L0}Tem cells communicate with FoxP3⁺ Tregs to synergistically produce IL-10 (Figs 3-4). To confirm that the increase in IL-10 originated from FoxP3⁺ Tregs in these experiments, we cultured Tregs and Rb^{L0}Tem cells alone or together as before, only using Rb^{L0}Tem cells from IL-10-knockout (IL-10ko) mice. ELISA of IL-10 showed that FoxP3⁺ Tregs produce almost no IL-10 when cultured alone, but the inclusion of IL-10ko Rb^{L0}Tem cells dramatically increased IL-10 concentration (Fig 5A). These data show that the Rb^{L0}Tem cells induce FoxP3⁺ Tregs to produce IL-10.

In order to determine the contact dependence of this communication, we measured FoxP3⁺ Treg IL-10 output *in vitro* after co-culturing with either

paraformaldehyde-fixed Rb^{L0}Tem or Rb^{Hi}Tn cells, or by supplementation of FoxP3⁺ Treg media with conditioned media from stimulated Rb^{L0}Tem or Rb^{Hi}Tn cells. We found that fixation of the Rb^{L0}Tem cells eliminated the synergy (Fig 5B), while Rb^{L0}Tem-conditioned media was able to robustly induce IL-10 production in live FoxP3⁺ Tregs (Fig 5C). In addition, neutralizing antibody blockade of the Sema4-Neuropilin cell contact pathway reported to promote Treg activity [102] also did not reduce the synergistic production of IL-10 (Fig 12). These data suggest that Rb^{L0}Tem cells communicate with Tregs via a soluble mediator(s). To confirm that conditioned media from Rb^{L0}Tem cells also lead to IL-10 production *in vivo*, we induced pulmonary inflammation in IL-10-GFP reporter mice using lung house dust mite antigen (HDM) challenges and then intranasally administered conditioned media from either Rb^{L0}Tem or Rb^{Hi}Tn cells, with untreated HDM mice and resting mice as controls. As seen *in vitro* (Fig 5C), we found that Rb^{L0}Tem but not Rb^{Hi}Tn conditioned media significantly increased the percentage of IL-10-producing CD4⁺ T cells in the airway compared to untreated HDM-inflamed mice (Figs 5D-E). Although resting mice had too few CD4⁺ T cells for robust analysis of their IL-10 expression pattern, there was no difference in the total number of CD4⁺ T cells in all HDM-challenged mice (Fig 5E). Thus, a soluble mediator(s) produced by Rb^{L0}Tem but not Rb^{Hi}Tn cells can induce IL-10 in FoxP3⁺ Tregs *in vitro* and in recipient lung CD4⁺ T cells *in vivo*.

Treg suppressive activity was measured in co-cultures of WT FoxP3⁺ Tregs and WT Rb^{L0}Tem cells for 4 days with anti-CD3 ϵ antibody stimulation. The presence of FoxP3⁺ Tregs significantly reduced the activation state of the Rb^{L0}Tem cells,

as measured by IFN γ ELISA, supporting the conclusion that the Tregs are active and suppressive (Fig 5F).

3.4.4 The Rb^{Lo}Tem transcriptome

In order to identify the mediator(s), we compared the transcriptomes of anti-CD3 ϵ activated Rb^{Lo}Tem and Rb^{Hi}Tn cells by mRNA deep sequencing (RNAseq). We arranged the change in copy number by the ratio of Rb^{Lo}Tem to Rb^{Hi}Tn RPKM values because we predicted that the mediator must be significantly up-regulated in the Rb^{Lo}Tem population relative to the Rb^{Hi}Tn population. Lead candidates were robustly transcribed (RPKM > 2), at least 16-fold greater in Rb^{Lo}Tem over Rb^{Hi}Tn cells, and known to be secreted (*i.e.*, non-membrane proteins; not found in the nucleus or cytoplasm). This analysis revealed a list of highly up-regulated genes which might account for the activity of these cells, including IFN γ , IL-4, IL-22 and others (Fig 6).

3.4.5 Neutralization of IL-4 eliminates IL-10 synergy

In order to identify the molecules mediating T cell synergy, we performed antibody neutralization experiments during co-culture of FoxP3⁺ Treg and Rb^{Lo}Tem cells based on the transcriptomic data (Fig 6). We found that neutralization of IL-4 eliminated the synergistic production of IL-10 (Fig 7A). In repeat experiments comparing neutralization of IL-4 to neutralization of IL-4R α (CD124), which inhibits both type I and type II IL-4 receptor complexes, we found

a corresponding elimination of IL-10 synergy (Fig 7B). To identify which cell the IL-4 was impacting, we neutralized CD124 on only the Rb^{L0}Tem cells by pre-incubation with the antibody, washing away unbound antibody, then co-culturing the CD124-blocked Rb^{L0}Tem cells with fresh FoxP3⁺ Tregs. We found no difference in IL-10 synergy (Fig 7C). However, the inverse experiment in which the FoxP3⁺ Tregs were pre-blocked with anti-CD124 revealed robust inhibition of synergy (Fig 7D). Moreover, we tested the impact of IL-4 neutralization in FoxP3⁺ Treg mono-cultures using conditioned media from Rb^{L0}Tem cells. Once again, we found that blockade of IL-4 eliminated the IL-10 response (Fig 7E).

In order to determine whether IL-4 was necessary and/or sufficient to induce IL-10 in Tregs, we cultured FoxP3⁺ Tregs with fresh media supplemented with recombinant IL-4 (rIL-4) and IL-2 (rIL-2) together and independently. Although our data already demonstrated that IL-2 was not the primary driver of IL-10 production (Figs 3D & 3F), IL-2 was used because IL-2 concentrations robustly decrease in co-culture (Fig 3D), suggesting that it may play the well-documented pro-survival role for Tregs [103]. We found that rIL-4 induced IL-10 in mono-cultured FoxP3⁺ Tregs, but that the addition of IL-2 greatly enhanced this response despite the failure of IL-2 to robustly induce IL-10 in the absence of IL-4 (Fig 7F). This effect was dependent upon CD124, since neutralizing antibody completely reversed the impact of rIL-4 supplementation (Fig 7F). Cytokine titration experiments with isolated FoxP3⁺ Tregs and varied concentrations of rIL-2 (Fig 7G) and rIL-4 (Fig 7H) further demonstrated the dose-response nature of

IL-10 production downstream of exposure to these cytokines. We also found that the expression of CD124 in FoxP3⁺ Tregs was dependent upon prior stimulation with α CD3 ϵ antibody, and this expression was not impacted by the presence of Rb^{Lo}Tem cells (Fig 7I-7J).

3.4.6 Rb^{Lo}Tem cells require IL-4 to protect mice from pulmonary inflammation

The *in vitro* experiments implicate Rb^{Lo}Tem cells as a key population of T cells capable of inducing IL-10 release by FoxP3⁺ Tregs, while transcriptomic and antibody-mediated neutralization experiments implicated a dependence upon IL-4 to promote this response. In order to test the Rb^{Lo}Tem protective activity and their dependence on IL-4 *in vivo*, we performed an adoptive transfer experiment into a house dust mite (HDM)-induced acute asthma model. Rb^{Lo}Tem cells were isolated as before (Fig 11) from either WT or IL-4 knockout (IL-4ko) mice, stimulated *in vitro* for 48 hours with anti-CD3 ϵ antibody, then transferred via the tail vein into recipient WT mice on day 7 of HDM challenges. Robust immune suppression, as measured by the total number of airway-infiltrating leukocytes (Fig 8A), overall clinical score (Fig 8B; Table 1), neutrophils, lymphocytes, macrophages and eosinophils (Fig 8C) recovered in bronchoalveolar lavage fluid (BALf), was achieved with a single transfer of 60,000 WT cells. Moreover, tissue pathology measured by confocal microscopy for activated leukocytes (Fig 8D) and hematoxylin and eosin staining (H&E; Fig 9) was returned to baseline in mice receiving WT Rb^{Lo}Tem cells, while TriChrome and periodic acid-Schiff (PAS) staining revealed a reversal of collagen deposition (i.e. tissue remodeling) and mucus production, respectively (Fig 9). Importantly, this potent ability to

reverse lung inflammation was lost when the Rb^{Lo}Tem cells lacked IL-4 (Figs 8-9), confirming the central role for IL-4 in Rb^{Lo}Tem-mediated immune suppression.

Parameter	Score	Description
Hyperplasia	0	None
	1	Not more than 2 bronchi with mild to moderate epithelial hyperplasia
	2	Many bronchi with moderate hyperplasia
	3	Most bronchi with moderate to severe hyperplasia
Infiltration	0	None
	1	Small numbers of infiltrating immune cells (undifferentiated)
	2	Moderate numbers of infiltrating immune cells
	3	High numbers of infiltrating immune cells
Localization	0	Infiltrating cells limited to one or two bronchi
	1	Infiltrating cells seen around a plurality of bronchi
	2	Infiltrating cells seen around all bronchi and some dissemination in the alveolar space
	3	Infiltrating cells throughout the tissue

Table 1. Lung inflammation clinical score rubric.

H&E stained lung sections were scored for epithelial cell hyperplasia, infiltration of immune cells, and localization of immune cells on a zero to 3 scale for each parameter. Final clinical scores were the sum of each parameter for each tissue

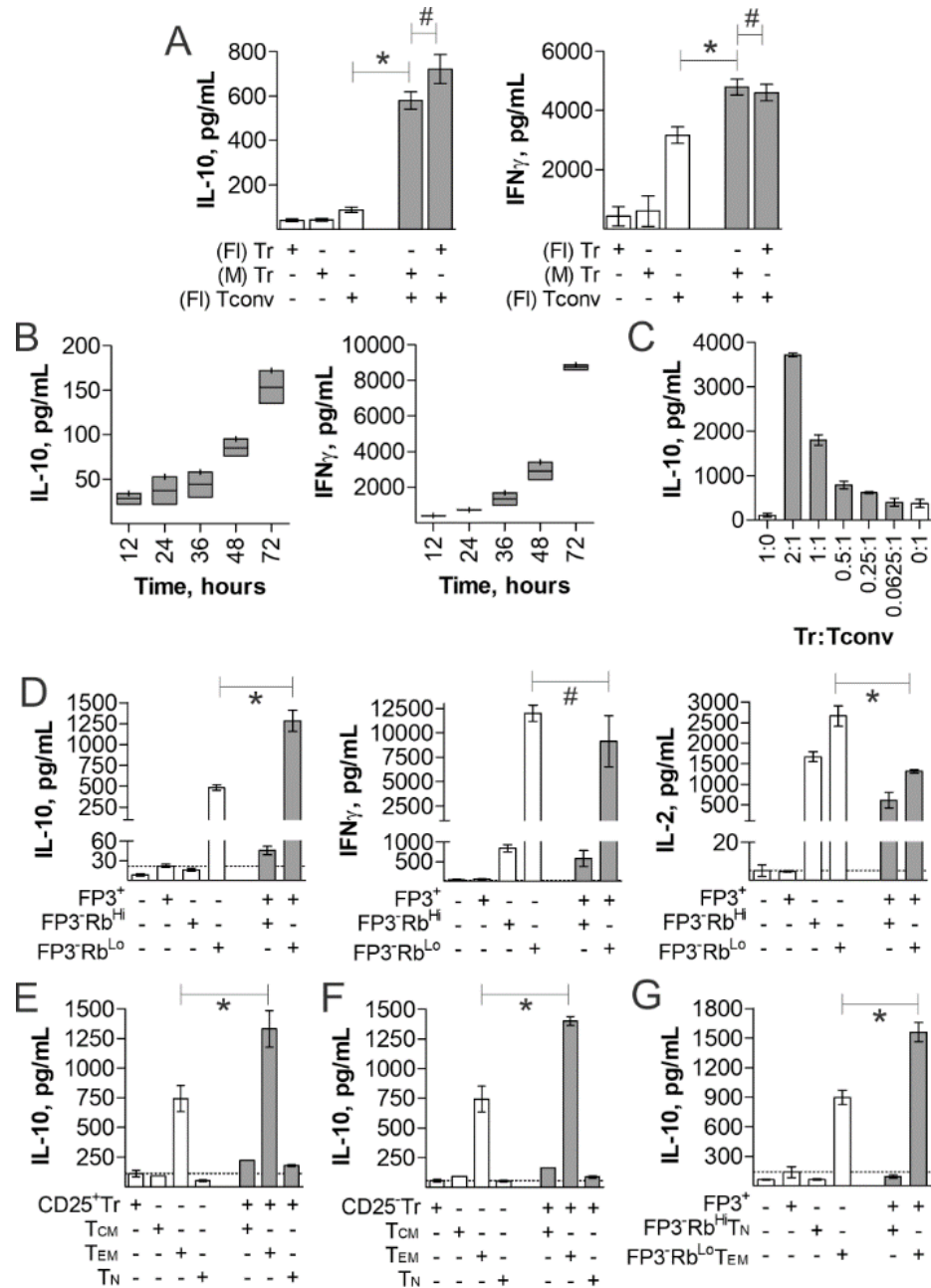


Figure 3. IL-10 production by Tregs is synergistically enhanced by CD4⁺FoxP3⁻CD45Rb^{Lo}CD44⁺CD62L⁻ T cells. Tregs and various CD4⁺ T cell subsets were cultured *in vitro* with plate-bound anti-CD3ε antibody for 3 days, unless otherwise specified, to measure their cytokine responses by ELISA. (A) Comparison of mono- and co-cultures of magnetic bead purified (M) CD4⁺ Tconv and CD4⁺CD25⁺ Tr cells vs. flow sorted (FI) CD4⁺CD25⁺ Tr cells. (B) Time course of cytokine production from co-cultures of flow-sorted Tconv and CD25⁺ Tregs. (C) Co-cultures of flow-sorted 50k Tconv and varied Tregs at indicated ratios. (D) 1:1 Cultures of flow sorted CD4⁺FoxP3⁺ Tregs and CD4⁺FoxP3⁻CD45Rb^{Lo} cells, showing IL-10, IFN γ , and IL-2 production by ELISA. (E) 1:1 cultures of CD4⁺CD25⁺FoxP3⁺ Tregs and CD4⁺CD25⁻FoxP3⁻CD62L⁻CD44⁺ (Tcm), CD4⁺CD25⁻FoxP3⁻CD62L⁻CD44⁺ (Tem), and CD4⁺CD25⁻FoxP3⁻CD62L⁻CD44⁺ (Tn) cells. (F) 1:1 cultures of CD4⁺CD25⁻FoxP3⁺ Tregs and Tcm, Tem, or Tn cells. (G) 1:1 cultures of CD4⁺FoxP3⁺ Tregs and CD4⁺FoxP3⁻CD45Rb^{Lo}CD62L⁻CD44⁺ (Rb^{Lo} Tem) or CD4⁺FoxP3⁻CD45Rb^{Hi}CD62L⁻CD44⁺ (Rb^{Hi} Tn) cells. * = p<0.05; # = p>0.05. P value calculated from Student's T-Test. Error bars show mean with SEM. For A and D-F, n=3 experiments. For C, n=6 experiments. For G, n=4 experiments.

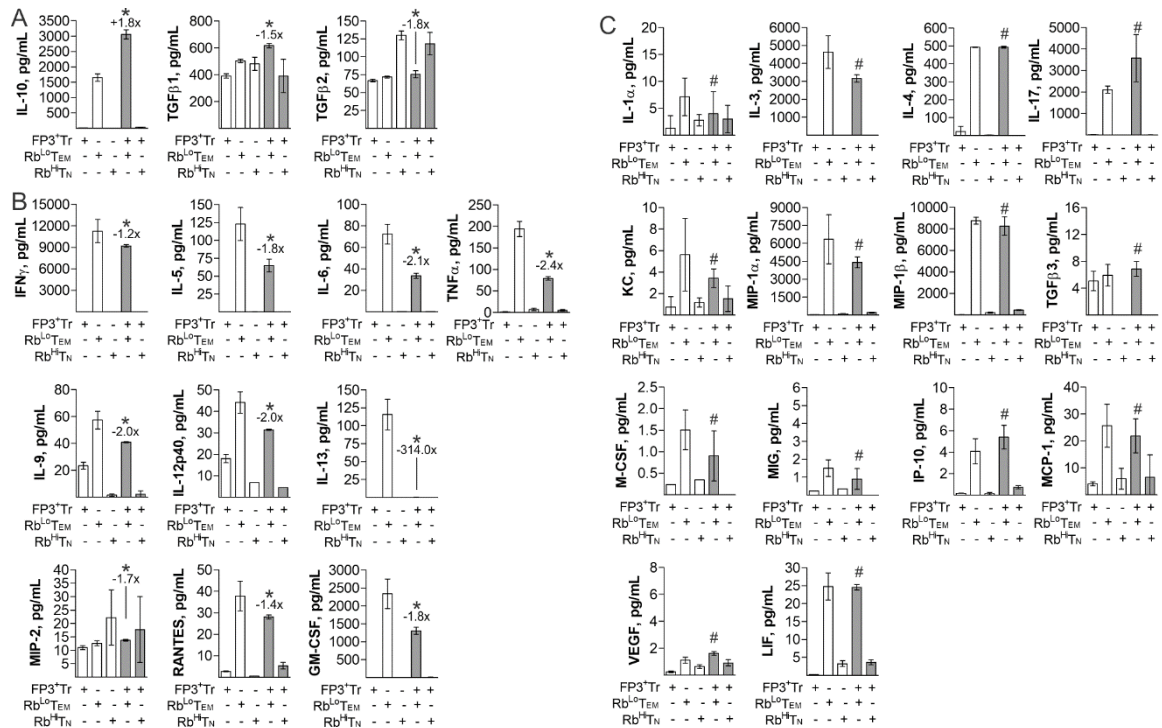


Figure 4. Cytokine synergy of Rb^{Lo} Tem and FoxP3⁺ Tregs is limited to IL-10. Rb^{Lo} Tem and Rb^{Hi} Tn cells were stimulated alone or in co-culture as before for 3 days to determine cytokine and chemokine secretion in relation to the mRNA transcriptomes using multiple Luminex. Statistical comparisons were made based on differences between the sum of the FoxP3⁺ Treg and Rb^{Lo} Tem individual responses and the corresponding co-culture. Shown are immune regulation-associated proteins with significant change in co-culture (A), other cytokine and chemokines with statistically significant differences in co-culture (B), and molecules not significantly different in co-culture (C). * = p<0.05; # = p>0.05. P value calculated from Student's T-Test. Error bars show mean with SEM. n=3 experiments for all panels.

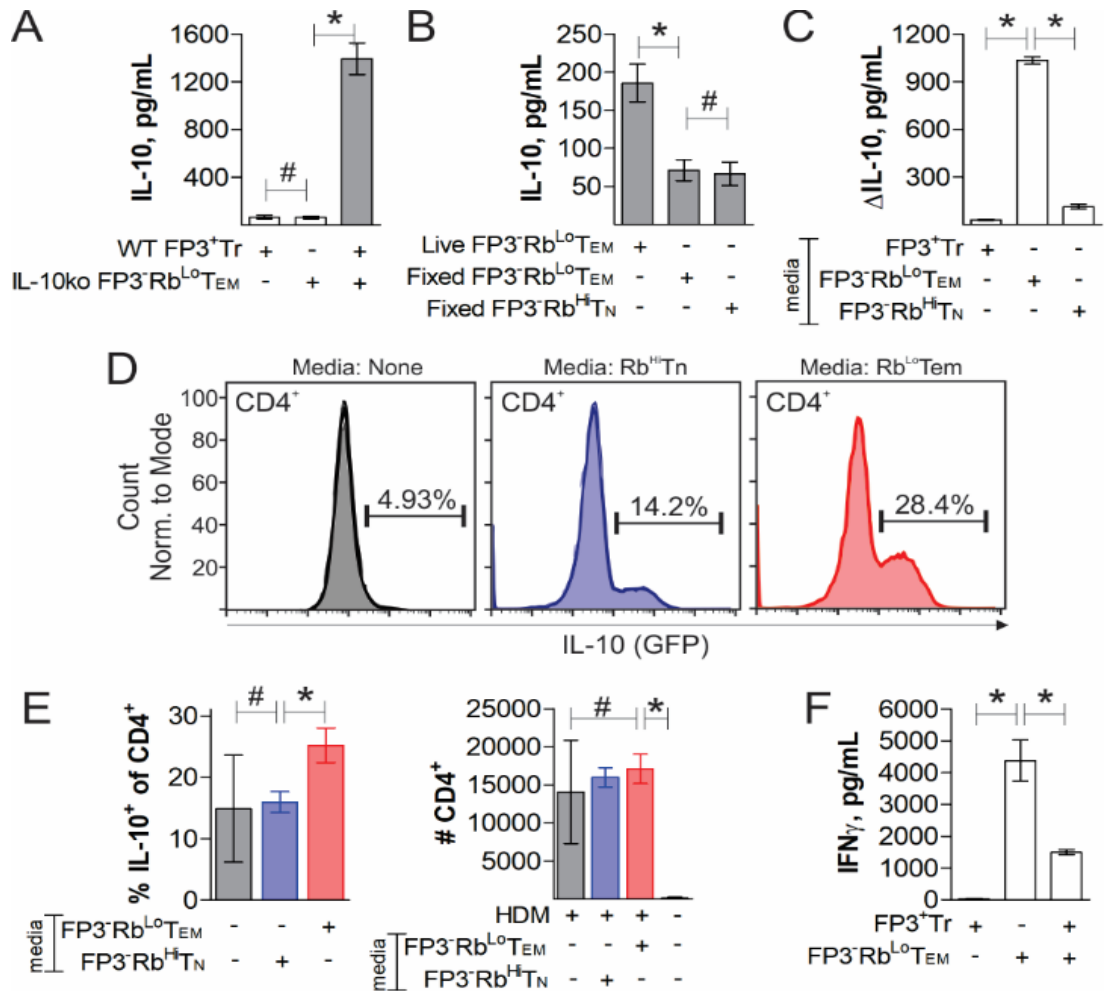


Figure 5. T cell synergy is mediated by a soluble factor. Cells were flow sorted, stimulated with anti-CD3 ϵ antibody for 3 days, and treated as indicated. ELISA measurements of IL-10 concentration in culture supernatant from FoxP3⁺ Tregs co-cultured with IL-10-knockout Rb^{Lo} Tem (A), fixed Rb^{Lo} Tem or Rb^{Hi} Tn cells (B) or the change in IL-10 in the supernatant from cultured FoxP3⁺ Tregs supplemented with conditioned media from Rb^{Lo} Tem, Rb^{Hi} Tn or FoxP3⁺ Tregs stimulated previously for 3 days as before (C). Conditioned media from activated Rb^{Lo} Tem or Rb^{Hi} Tn cells were administered to HDM-challenged IL-10-GFP reporter mice intranasally and compared to resting and HDM-challenged mice without conditioned media. Mice were sacrificed and the BALf was analyzed by flow cytometry, showing percent IL-10⁺ among CD4⁺ cells in representative histograms (D) as well as replicates and the total CD4⁺ cell counts (E). ELISA measurements of IFN γ concentration in culture supernatants from FoxP3⁺ Tregs, WT Rb^{Lo} Tem, or both cells in co-culture with anti-CD3 ϵ stimulation for 4 days (F). * = p<0.05; # = p>0.05. P value calculated from Student's T-Test. Error bars show mean with SEM. For A-C, n=3 to 6 experiments. For E-F, n=3 experiments.

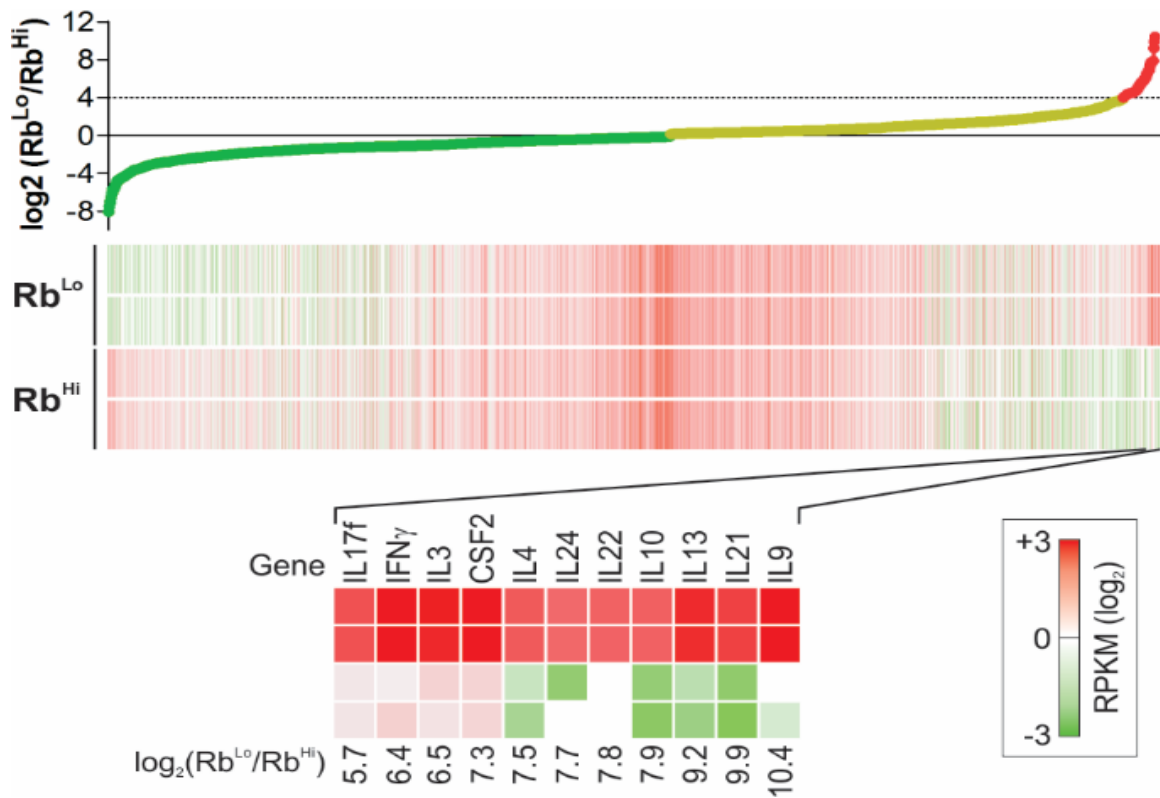


Figure 6. $\text{Rb}^{\text{Lo}}\text{Tem}$ and $\text{Rb}^{\text{Hi}}\text{Tn}$ transcriptomes reveal potential crosstalk mediators. $\text{Rb}^{\text{Lo}}\text{Tem}$ and $\text{Rb}^{\text{Hi}}\text{Tn}$ cells were stimulated alone as before for 3 days, and RNA was isolated for deep sequencing and whole transcriptome analysis. Genes were arranged according to the \log_2 of the $\text{Rb}^{\text{Lo}}\text{Tem}$ to $\text{Rb}^{\text{Hi}}\text{Tn}$ ratio of expression, using the calculated RPKM values. Candidates were narrowed by excluding all membrane proteins, proteins known to exist only in the nucleus or cytoplasm, and those showing at least 16-fold increase in $\text{Rb}^{\text{Lo}}\text{Tem}$ cells compared to $\text{Rb}^{\text{Hi}}\text{Tn}$ cells. $n=2$ per cell type.

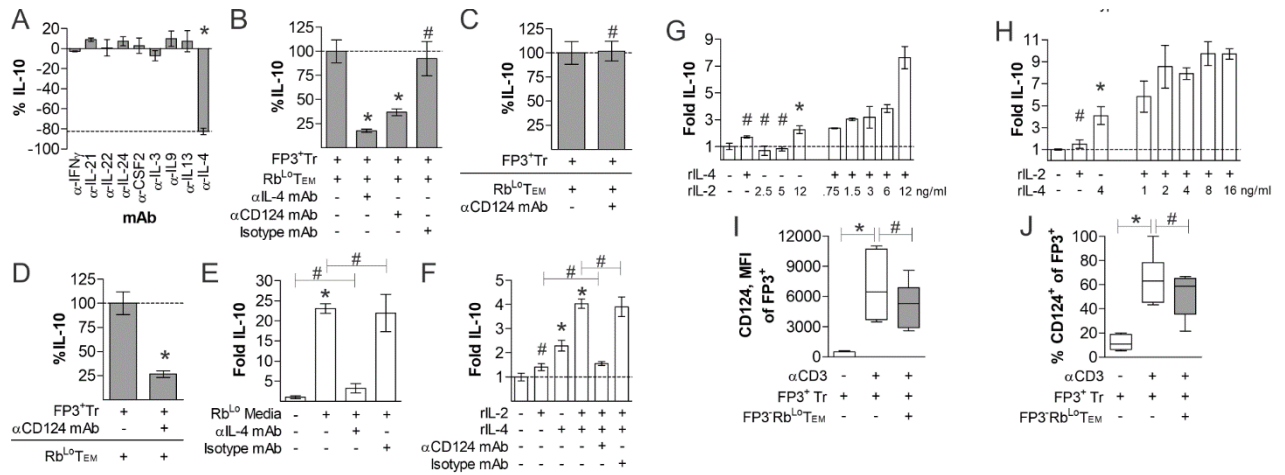


Figure 7. IL-4 and FoxP3⁺ Treg IL-4Rα (CD124) mediates Treg IL-10 production. FoxP3⁺ Tregs and Rb^{Lo} Tem were stimulated in co-culture as before for 3 days with the addition of cytokine (A) or receptor (B) neutralizing antibodies to identify the mediator of IL-10 synergy. (C) To determine whether IL-4 was acting on Rb^{Lo} Tem cells or FoxP3⁺ Tregs, (C) Rb^{Lo} Tem cells were incubated with CD124 neutralizing antibody, washed, then co-cultured with fresh FoxP3⁺ Tregs as before (C); and then compared to pre-incubating FoxP3⁺ Tregs with CD124 antibody followed by co-culture with Rb^{Lo} Tem cells (D). FoxP3⁺ Tregs were stimulated as before in monoculture supplemented with either conditioned media from stimulated Rb^{Lo} Tem cells (E) or various concentrations, denoted in ng/mL, of recombinant IL-2 or IL-4 (F-H) with and without neutralizing IL-4 or CD124 antibodies (E-H). (I-J) FoxP3⁺ Tregs were cultured with and without αCD3ε stimulation, as well as with and without Rb^{Lo} Tem cells. At day 3, cells were harvested and stained for CD124 expression, and analyzed by geometric mean fluorescence intensity (I) and the percent CD124 positive among FoxP3⁺ Tregs (J). * = p<0.05; # = p>0.05. P value calculated from Student's T-Test, with comparisons to control unless specified. Error bars show mean with SEM. For A-H, n=3 to 6 experiments. For I-J, n=6 experiments.

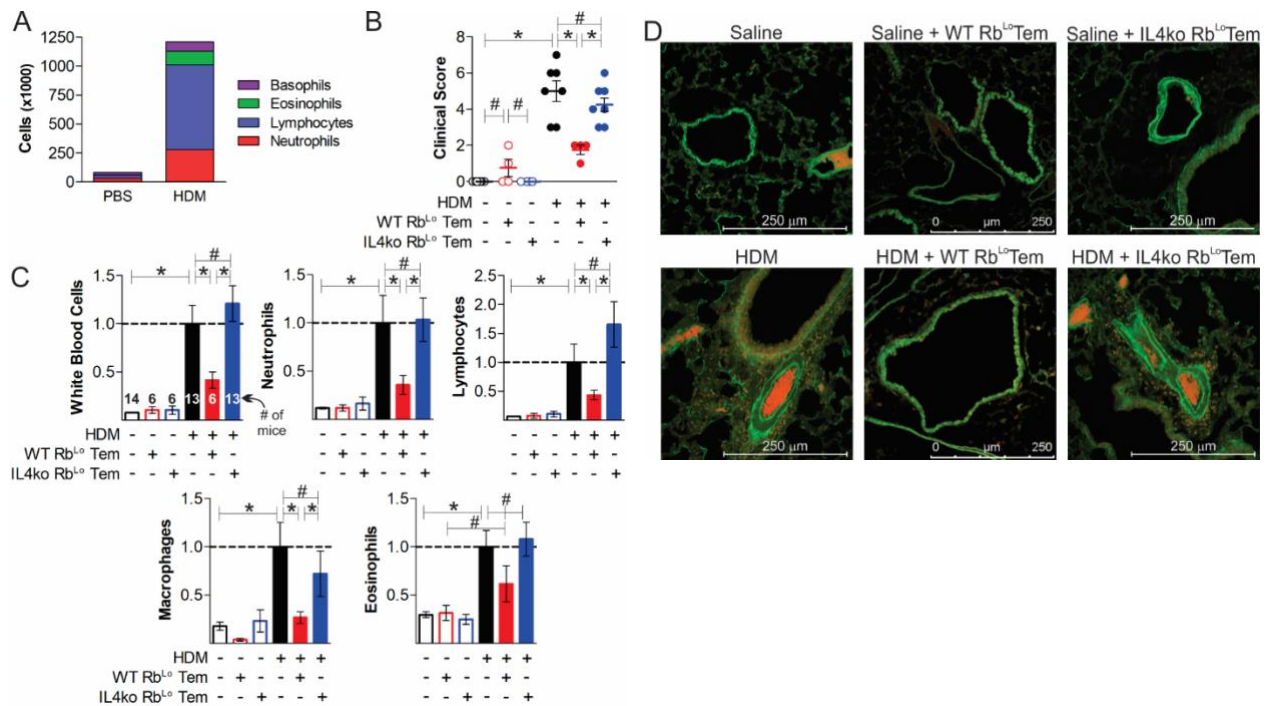


Figure 8. Rb^{Lo} Tem cells reverse lung inflammation in an IL-4-dependent fashion. Mice were given 60,000 of anti-CD3 ϵ -stimulated WT or IL-4ko Rb^{Lo} Tem cells on day 7 of acute HDM-induced asthma to test their ability to reverse inflammatory pathology. The total number of infiltrating cells (A), the clinical score (see Table 1) (B), normalized cellular differentials from BALf harvests (C), and tissue pathology (D) by immunofluorescence staining for EpCAM (green) and MPO (red) from representative sections of pulmonary tissue are shown. * = $p < 0.05$; # = $p > 0.05$. P value calculated from an unpaired Student's T-Test. Error bars show mean with SEM. $n = 6$ to 14 individual mice total per group, across two asthma trials, as indicated on the White Blood Cell counts in panel C.

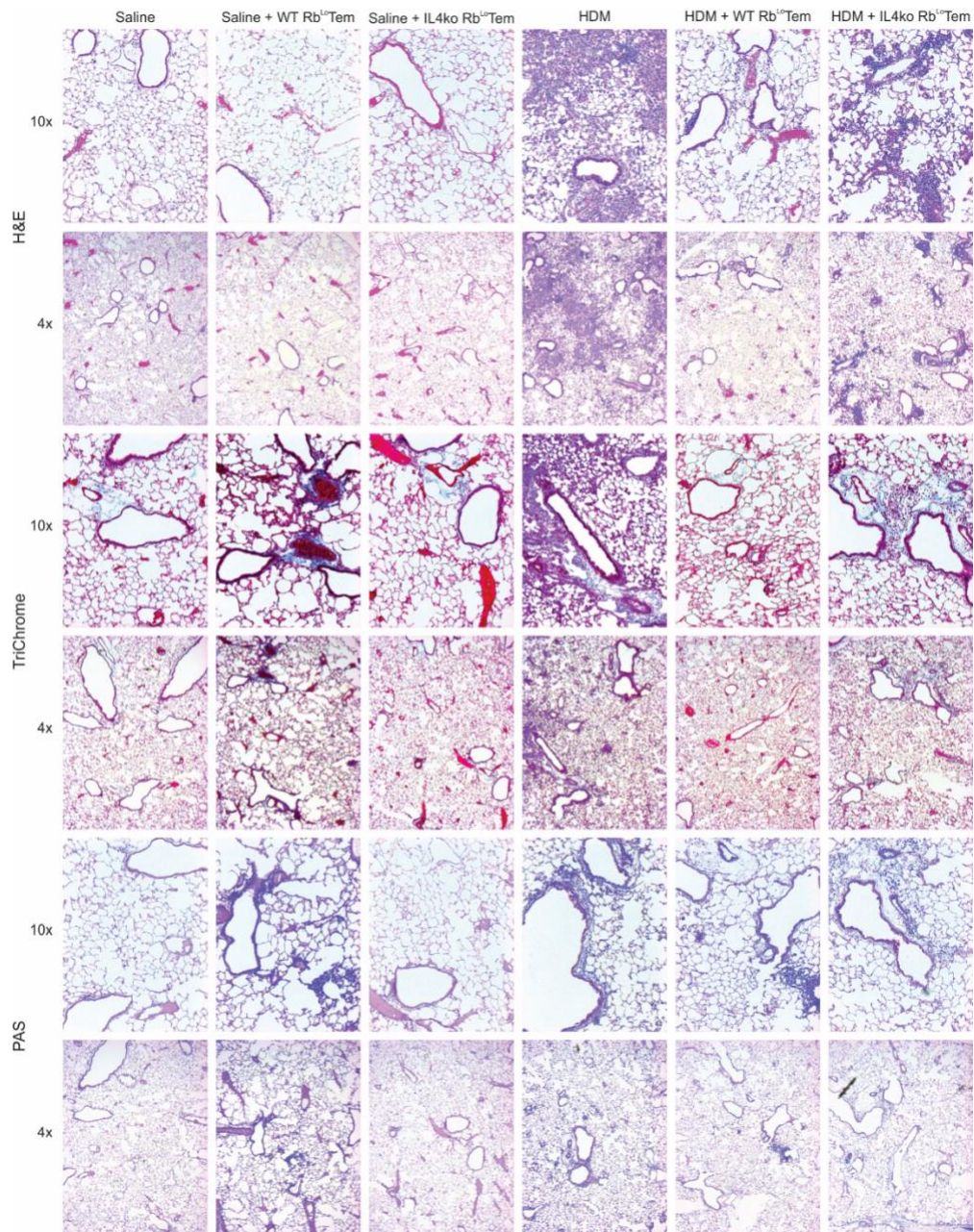


Figure 9. Lung inflammation, remodeling and mucus production is reversed by Rb^{Lo}Tem cells in an IL-4-dependent fashion. Representative lung sections from n=6 mice at 4x and 10x magnification from the mice described in Fig 6 were stained with H&E (top), TriChrome (middle) and PAS (bottom) to assess cellular infiltration, tissue remodeling/collagen deposition and mucus production respectively in HDM-challenged mice receiving 60,000 activated WT or IL-4ko Rb^{Lo}Tem cells.

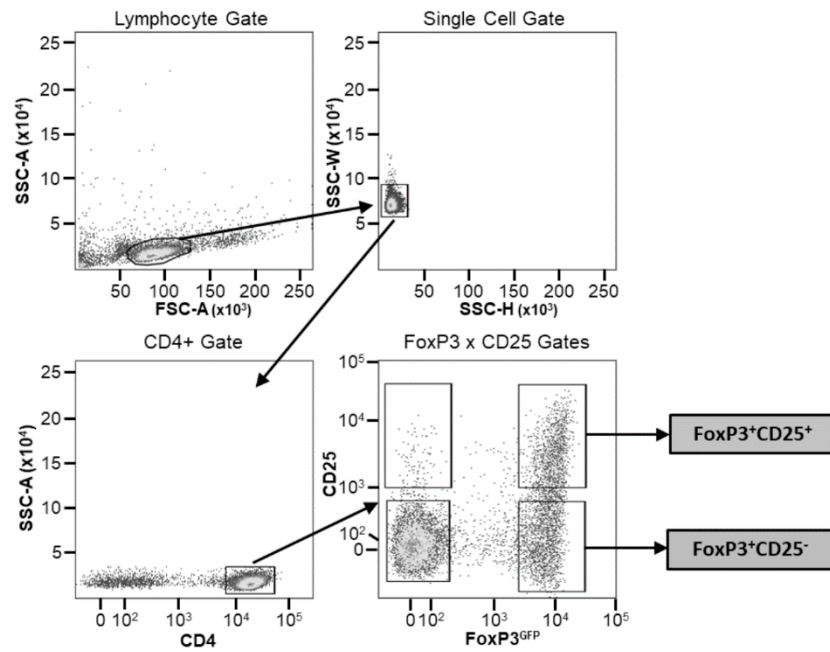


Figure 10. Flow setup for sorting Tregs based on CD25. Experimental design for the gating strategy utilized to capture CD4⁺FoxP3⁺CD25⁺ and CD4⁺FoxP3⁺CD25⁻ cells from magnetically sorted splenocytes from FoxP3-RFP reporter mice.

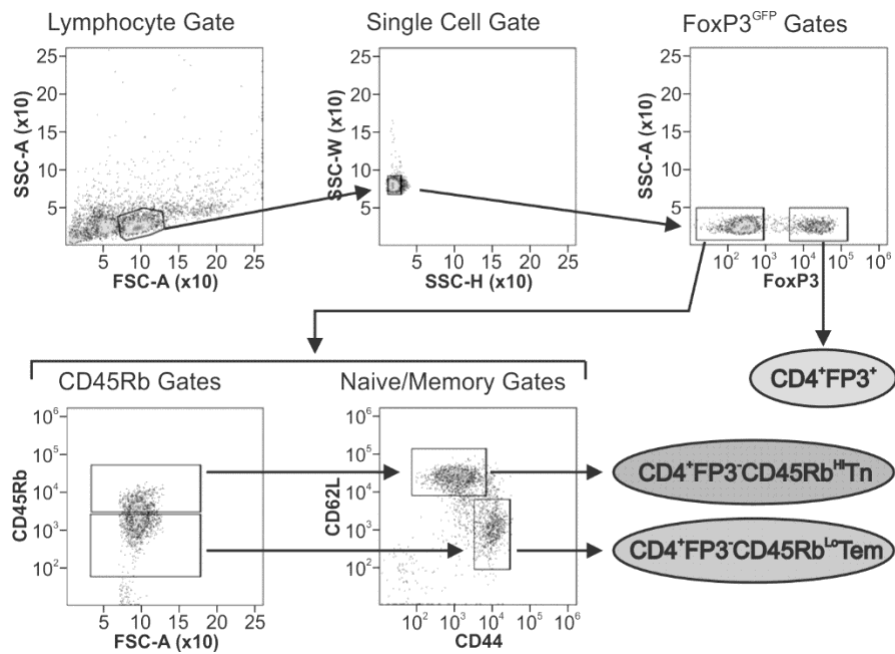


Figure 11. Flow setup for sorting T cell subpopulations. Experimental design schematic detailing the staining and gating strategy used to isolate CD4⁺FoxP3⁺, CD4⁺FoxP3⁻CD45Rb^{Lo}CD44⁺CD62L⁻, and CD4⁺FoxP3⁻CD45Rb^{Lo}CD44⁺CD62L⁻ cells from CD4⁺ magnetically sorted splenocytes.

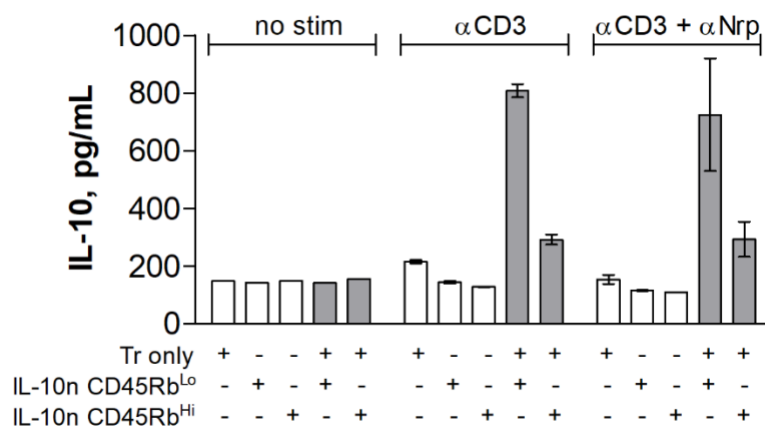


Figure 12. Blocking neuropilin1 does not engage IL-10 production in Tregs. ELISA measurements of IL-10 in mono- and co-culture supernatants after 72h from FoxP3⁺ Tregs or CD4⁺CD45Rb^{Lo} and CD4⁺CD45Rb^{Hi} cells from IL-10n animals. Cells were grown with or without stimulus from plate-bound αCD3ε and supplementation with a blocking αNeuropilin1 antibody. Error bars show mean with SEM.

**Chapter 4: Characterization of Polysaccharide A Response Reveals
Interferon Responsive Gene Signature and Immunomodulatory Marker
Expression**

4.1 Abstract

Polysaccharide A (PSA), a capsular carbohydrate from the commensal gut bacteria *Bacteroides fragilis*, has been shown to possess both potent T cell-dependent pro- and anti-inflammatory properties. PSA is able to induce abscess and adhesion formation in sepsis models, but can also inhibit asthma, inflammatory bowel disease (IBD) and experimental autoimmune encephalomyelitis (EAE) through MHCII-dependent activation of CD4⁺ T cells. Yet, despite decades of study, the ability of PSA to balance both these pro- and anti-inflammatory responses remains poorly understood. Here we utilized an unbiased systems immunology approach consisting of RNAseq transcriptomics, high-throughput flow cytometry and Luminex analysis to characterize the full impact of PSA-mediated stimulation of CD4⁺ T cells. We found that exposure to PSA resulted in the upregulation and secretion of IFN γ , TNF α , IL-6 and CXCL10, consistent with an interferon responsive gene (IRG) signature. Importantly, PSA stimulation also led to expression of immune checkpoint markers Lag3, Tim3 and especially PD1, which were also enriched and sustained in the gut associated lymphoid tissue of PSA-exposed mice. Taken together, PSA responding cells display an unusual mixture of pro-inflammatory cytokines and anti-inflammatory surface receptors, consistent with the ability to both cause and inhibit inflammatory disease.

4.2 Introduction

Humans have evolved a complex relationship with colonizing bacteria in which the bacteria and their components play a key role in establishing tolerance and maintaining homeostasis. Indeed, dysbiosis of the gut microbiome is linked to autoimmunity [104, 105], hyper responsive disorders [106] and cancer development [107, 108], while use of commensal bacteria or their components can reduce disease burden [109-112].

Bacteroides fragilis is a gram negative and naturally occurring member of the normal human microbiota, and has been robustly demonstrated to have both pro- [113] and anti-inflammatory [67, 68, 110] effects in rodents. This activity is mediated primarily by its capsular carbohydrate polysaccharide A (PSA) through its ability to elicit a strong T cell response [76] following processing via TLR2-stimulated nitric oxide production [114] and subsequent presentation by canonical class II MHC (MHCII) in a glycosylation-dependent fashion [34, 115]. Interestingly, *B. fragilis* was originally identified and characterized as the most common anaerobic isolate from intra-abdominal abscesses [62], with the capsular complex being the key T cell stimulator required for this inflammatory and fibrotic response [76]. However, it was later discovered that PSA could also prevent those same abscesses if the animal was exposed to purified PSA prior to abscess induction [116]. This initial discovery of an anti-inflammatory role has now been expanded to include the ability to protect against inflammatory models such as adhesion formation [117], asthma [67], IBD [74], and EAE [110].

Research focused upon the PSA-responsive T cell population has established that PSA exposure leads to the clonal expansion [35] of a subset of CD4⁺CD45Rb^{low}CD62L⁻CD44⁺FoxP3⁻ T effector/memory (Rb^{L0}Tem) cells [68, 118]. These cells suppress asthmatic inflammation in an IL-10-dependent fashion in cooperation with tissue-resident regulatory T cells (Tregs), whereby Tregs are selectively induced to release IL-10 when Rb^{L0}Tem cells are present [68, 118]; however, the PSA-stimulated Rb^{L0}Tem cells are also strong producers of IFN γ , the canonical pro-inflammatory cytokine of T helper type 1 cells (Th1)[119]. Given the acknowledged importance of the microbiota in the maintenance of homeostasis, and the potent and complex T cell stimulatory properties of PSA, we sought to generate a more complete characterization of the T cells activated and expanded by PSA through a combination of deep RNA sequencing transcriptomics, high throughput flow cytometric quantitation of surface proteins, and multianalyte Luminex analyses of secreted cytokines and chemokines. We found that PSA induces the upregulation and expression of numerous immunological genes and molecules associated with an interferon responsive gene (IRG) signature, as well as transcription factors such as T-bet, signal transducer and activator of transcription (STAT) 1, and STAT4 which are associated with a Th1 phenotype [119, 120]. Interestingly, T cell surface marker examination revealed the upregulation of immune-regulatory markers such as Tim3, Lag3, and especially PD1 in response to PSA, collectively pointing towards a regulatory phenotype. Together with *in vivo* validation of these changes within the gut-associated lymphoid tissue (GALT) of orally PSA-exposed mice, these

results show the PSA response is primarily driven by interferon but is phenotypically both anti- and pro-inflammatory, suggesting that the overall immunologic outcome of PSA exposure is highly context dependent. These data help to better understand the true nature of our relationship with the glycome of commensal microbes like *B. fragilis* which are known to provide strong systemic immunologic benefit under homeostatic circumstances [67, 110, 112, 116, 118, 121], while causing inflammation if they breach the normal gut compartment [62, 109, 113].

4.3 Methods

4.3.1 Mice.

C57BL/6J (Stock #000664), FoxP3 RFP (C57BL/6-FoxP3 tm1Flv /J, Stock #008374 mice, all on the C57BL/6 background were purchased from the Jackson Laboratory (Bar Harbor, ME). Mice were housed in a 12 hr light/dark cycle specific pathogen free facility and fed standard chow (Purina 5010) ad libitum. Enrichment and privacy were provided in mating cages by 'breeding huts' (Bio-Serv S3352-400). Mouse studies and all animal housing at Case Western Reserve University were approved by and performed according to the guidelines established by the Institutional Animal Care and Use Committee of CWRU.

4.3.2 PSA Purification

PSA was isolated from 20L of log-phase *B. fragilis* culture, using the NCTC9343 *B. fragilis*-derived $\Delta 44$ strain expressing only PSA [77] exactly as previously described [122]. Purity was determined by SDS-PAGE, BCA assay for protein, and absorbance scans for protein and nucleic acid.

4.3.3 Primary Splenic, Peyer's Patch and Mesenteric Lymph Node T Cells

Primary splenocytes were isolated from freshly harvested spleens, Peyer's patches or mesenteric lymph nodes and reduced to a single cell suspension by passing them through a sterile 100 μ M nylon mesh cell strainer (Fisher Scientific, Hampton, NH). For splenic T cell sorting, single cell suspension were labeled with anti-mouse CD4 magnetic microbeads (Miltenyi Biotec, San Diego, CA), and separated with an autoMACS Pro Separator (Miltenyi Biotec, San Diego, CA), per manufacturer's instructions.

4.3.4 Flow Cytometry and Cell Sorting

For splenic, Peyer's patch or mesenteric lymph node T cell flow cytometry, positively selected CD4⁺ cells were stained with combinations of antibodies (0.5 μ g/mL per) to Tim3-APC (BioLegend, San Diego, CA) or Lag3-APC (BD Bioscience), PD1-APC (BioLegend, San Diego, CA), CTLA4-APC (BioLegend, San Diego, CA), Ly6A/E-APC (BD Biosciences, San Jose, CA) and GITR-APC (BD Biosciences, San Jose, CA). Cells were washed twice in MACS buffer (Miltenyi Biotec, San Diego, CA) before analysis using Attune NxT

(ThermoFisher, Waltham, MA) with the support of the Cytometry & Imaging Microscopy Core Facility of the Case Comprehensive Cancer Center. Analysis of all FACS data was performed using FlowJo vX (Tree Star, Inc., Ashland, OR).

4.3.5 Cell Culture

After flow sorting, cells were cultured in 96-well plates (Corning, Corning, NY) at 50,000 cells per type per well in advanced RPMI (Gibco/Fisher Scientific, Waltham, MA) supplemented with 5% Australian-produced heat-inactivated fetal bovine serum, 55 μ M β -mercaptoethanol, 100U/mL and 100 μ g/mL Penicillin/Streptomycin, and 0.2mM L-glutamine (Gibco/Fisher Scientific, Waltham, MA) at 5% CO₂, 37°C.

4.3.6 ELISA, Blocking, Supplementation and Luminex

Cytokine levels were analyzed by standard sandwich ELISA performed by manufacturer's instructions (BioLegend, San Diego, CA), modified to utilize europium-conjugated streptavidin (Perkin-Elmer) detected with a Victor V3 plate reader (Perkin Elmer, San Jose, CA). Blocking experiments utilized antibodies to IFN- γ (10 μ g/mL, BioLegend, San Diego, CA). For IFN- γ blocking experiments, indicated cell types were incubated with 10 μ g/mL α IFN- γ at 4°C for 15 minutes, washed twice with PBS, then combined into co-culture. Supplementation assays were performed with recombinant mouse IFN- γ (BioLegend, San Diego, CA). For Luminex assays, media from indicated cultured populations were snap frozen in

liquid nitrogen and sent to Eve Technologies (Calgary, Ontario, Canada) for mouse 32-plex and TGF- β 3-plex analysis.

4.3.7 RNAseq and Analysis

For RNA sequencing, cells were harvested and washed twice in PBS. Pelleted cells were snap-frozen in liquid nitrogen and shipped to LC Sciences, LLC. for extraction, RNA purification and quality check, library creation and high-throughput sequencing (Illumina). Differential expression analysis and gene ontology was done using EdgeR v3.12.1 by LC Sciences, LLC. Genes showing significant differences (FDR >0.05 and log₂CPM >0) were selected for enrichment analysis using GAGE v2.20.1 by LC Sciences, LLC. We acknowledge our use of the gene set enrichment analysis, GSEA software, and Molecular Signature Database (MSigDB) [123] (<http://www.broad.mit.edu/gsea/>)

4.3.8 Data Analyses

All data are represented by mean \pm SEM. Data and statistical measurements were generated with GraphPad Prism (v5.0). For comparisons between two groups, Student's *t*-test was used; comparisons between multiple groups utilized analysis of variance.

4.4 Results

4.4.1 PSA-activated T cells show transcriptomic changes consistent with clonal expansion

We chose to examine the transcriptomic profile of PSA exposed murine CD4⁺ T cell splenocytes co-cultured with antigen presenting cells for 7 days *in vitro* (n= 3 per group). Using the least stringent analyses allowing for any significant ($p < 0.05$) non-zero (> 0 fold log₂CPM) change incorporating a false discovery rate (FDR) of < 0.05 , we identified over 16,000 differentially expressed genes (DEGs) relative to resting and unstimulated controls. Focusing upon the top 500 DEGs reveals clear groups of genes that are either up or down-regulated in response to PSA (Figure 13A). Using a multi-dimensional scaling plot (MDS) to provide a global view of gene expression, we found a remarkably high degree of similarity between PSA-exposed replicates (Figure 13B), reflecting the clonal expansion and transcriptomic programming of T cells responding to PSA. In contrast, resting and unstimulated CD4⁺ T cells showed a much higher degree of heterogeneity, as expected (Figure 13B). We also performed gene ontology (GO) analysis, where we found that the most enriched terms were mitotic cell cycle process (GO:1903047, Biological Process; Figure 13C), pyrophosphatase activity (GO:0016462, Molecular Function; Figure 13D), and mitochondrial part (GO:0044429, Cellular Component; Figure 13E), collectively pointing to a metabolically active proliferative state.

Closer examination of GO terms revealed an enrichment of immunological functions such as the cellular response to IFN γ (GO:0071346), response to IFN β (GO:0035458), cytokine activity (GO:0005125) and chemokine receptor binding (GO:0042379) (Figure 14A). Gene set enrichment analysis (GSEA) using the Hallmark gene sets [123, 124] and an FDR of < 0.25 showed 27 enriched sets

upon activation with PSA compared to control cells (Figure 14B). In parallel with the GO data, amongst the most highly enriched were interferon- α , interferon- γ and inflammatory response gene sets. (Figure 14C). When compared to the immunological signature c7 gene set from the Broad Institute [123, 124], there was strong enrichment in sets associated with tumor necrosis factor receptor (TNFR) and TNFR super family binding as well as IL-2 and STAT5 signaling pathways (Figure 14D). Moreover, the DEG profile favors iTreg (Figure 14E, left) over both nTreg and T conventional (Tc) cell profiles (Figure 14E).

4.4.2 PSA-responding T cells show an Interferon Responsive Gene (IRG) signature

GO and GSEA analysis showed a consistent enrichment in immunologic and interferon signaling, whether as a direct or indirect result of exposure to interferon molecules [119, 125, 126]. IRGs can be grouped depending on the type of interferon stimulation that induces their expression, including type 1 interferons (i.e. IFN α and IFN β) which can be produced by almost any cell upon viral infection [127], type 2 interferon (IFN γ), which is secreted by a number of leukocytes to combat infectious agents or cancer [119], and type 3 interferon (i.e. IFN λ), which is secreted by both leukocytes and epithelial cells [128]. In order to better categorize the PSA T cell response in terms of the apparent interferon response, we assembled a list of IRGs, including relevant cytokines, signaling molecules and markers associated with each type of interferon. We found 128 of the 215 IRGs were differentially expressed between PSA-activated T cells and control T cells (Figure 15A-15B). Dividing the list into its associated IFN types

further revealed clusters of upregulated and downregulated genes, although only IFN γ gene expression by RNA was observed (Figure 15C). This commonality in IRGs is likely due to the sharing of signaling machinery, such as Jak1/2, STAT1, and other IFN γ induced molecules, between the interferon types [126].

4.4.3 PSA-responding T cells show Th1-skewed signaling molecule and transcription factor expression

Next, we examined signaling molecules such as transcription factors, chemokines and cytokines to identify the nature of PSA-mediated T cell skewing. Focusing on T cell lineage-associated transcription factors, we found T-bet and FoxP3, commonly associated with Th1 and Treg populations respectively, were upregulated (Figure 16A). Conversely, ROR α , ROR λ t and GATA-3 were not enriched in PSA-responding cells.

Examination of STAT molecules showed a selective upregulation of STAT1 and STAT4, both of which are closely associated with IFN γ signaling (Figure 16B)[120, 126]. Similarly, the transcriptional expression of IFN inducible chemokines and receptors such as CXCR3, CCL5 and CCL2 (Figure 16C), combined with the upregulation of LIF, IL-1, and IL-6 (Figure 16D) are all consistent with the IRG signature of PSA.

4.4.4: Protein levels in PSA-responding T cells are consistent with an IRG signature

Thus far, our analyses have relied solely upon transcript levels measured by RNAseq; however, it is well known that the correlation between gene

transcription and protein concentration can be as little as 40%, depending on the system [129]. This is driven by differences in mRNA transcription rate and accessibility, translational control, intracellular trafficking and metabolism [129]. As a result, we first employed multianalyte Luminex analyses on secreted proteins from PSA-activated T cells and compared the result to the RNAseq data. As before, T cell and APC co-cultures were setup with or without PSA for 7 days. Culture media from these co-cultures were used to quantify 32 cytokines, chemokines and growth factors. A comparison of canonical cytokines associated with specific T helper lineages (Figure 17A) showed robust IFN γ release that was mirrored in the level of IFN γ transcript from RNAseq, further supporting a Th1-skewed phenotype. Interestingly, IL-4 protein (Th2-associated) was reduced with PSA exposure at day 7, although transcript levels were increased, possibly suggesting that IL-4 is being released, but is being taken up by neighboring cells [118]. For IL-9 (Th9) and IL-17 (Th17), both genes were not induced by PSA, while IL-10 (Treg) was reduced. Beyond these classical cytokines, we also found a number of other cytokines increased at the protein level, including IL-1, IL-6, IL-12 and CXCL10, although the mRNA transcript levels did not always reflect this increase (Figure 17B). Likewise, several cytokines were decreased in response to PSA at the protein level, including IL-2, IL-5 and IL-13 (Figure 17C), while still others did not change (Figure 18). As with IL-4, several molecules (i.e. IL-2, IL-5, IL-13, LIF, and CXCL5) were all increased at the mRNA level despite reductions in protein concentration.

For broad coverage of cell surface molecules, we employed the LegendScreen platform (Biolegend) to quantify 255 target proteins by flow cytometry after 1 or 7 days of PSA-mediated activation. The global profile of all markers on CD4⁺ T cells at day 0, 1 and 7 calculated from the geometric mean fluorescence (GeoMFI) shows a distinctive pattern of expression at both days 1 and 7 (Figure 19A). Examination of the top increased (Figure 19B) and decreased (Figure 19C) proteins revealed an increase in proliferation and activation markers such as CD44, Ly6A/E and CD255 [130-132], and decrease in other activation markers such as CD100 and CD27 [133, 134]. Interestingly, the data revealed six regulatory receptors (co-regulatory receptors) not previously associated with the PSA response, including Tim3, Lag3, and PD-1 (Figure 19D).

4.4.5: PSA-associated co-regulatory receptors are IRGs

The expression of PD-1 is strongly associated with suppression of the immune response, a phenomenon exploited by several cancers [135, 136]. Likewise, Tim3 and Lag3 have been shown to have important roles in immune suppression, usually in supportive roles of PD-1, leading to a synergistic upregulation of all three molecules [137, 138]. Given the strong IRG signature of the PSA T cell response, we sought to determine whether IFN γ would induce the expression of these co-regulatory receptors in PSA-naïve T cells. CD4⁺ T cells, or flow sorted CD4⁺ FoxP3⁻ T cells were cultured in the presence of anti-CD3 ϵ stimulation and supplemented with either recombinant IFN γ or anti-IFN γ neutralizing antibody for 3 days. We found that Tim3, Lag3, and PD-1 were all

increased in response to IFN γ , and this increase was ablated in the presence of IFN γ -neutralizing antibody (Figure 20A-B). Moreover, this was true for Lag3 and PD-1 in both bulk CD4⁺ splenocytes (Figure 20A-B) and cultures lacking Tregs (Figure 20C-D). Tim3 increases were lost in T cell populations lacking Tregs. This suggests that changes in Lag3 and PD-1 are primarily in Tc cells, while Tim3 is primarily in Tregs. Reduced IFN γ in these experiments demonstrated the efficacy of the neutralizing antibody (Figure 20B and 20D).

4.4.6: Co-regulatory receptors are increased within the GALT of PSA-exposed mice

All of the previous analyses indicate that exposure to PSA will lead to expression and production of IFN γ and a host of IFN γ -stimulated molecules, including co-regulatory receptors associated with immune suppression but not previously associated with PSA. In order to both validate the increased expression of these molecules, and to determine where they accumulate *in vivo*, CD4⁺ cells from mice orally exposed to PSA to mimic colonization with its source bacterium *B. fragilis* were harvested directly after the last PSA gavage (D17), 2 weeks after the last gavage (D31) or 5 weeks after the last gavage (D52). We found that our *in vitro* data was replicated *in vivo* in that the expression of activation markers Ly6A/E and GITR were increased on D31 in the gastrointestinal tract-associated lymphoid tissue (GALT), including both Peyer's patches (PP) and mesenteric lymph nodes (MLN) (Figure 21A). This trend was also seen for PD-1, CTLA4, Tim3 and Lag3 expression, with increased expression in the GALT on D31,

compared to any other time point (Figure 22B). Changes in the spleen were mild and generally failed to reach statistical significance, reflecting the potent local response to PSA when administered orally and validating the extensive *in vitro* analyses herein.

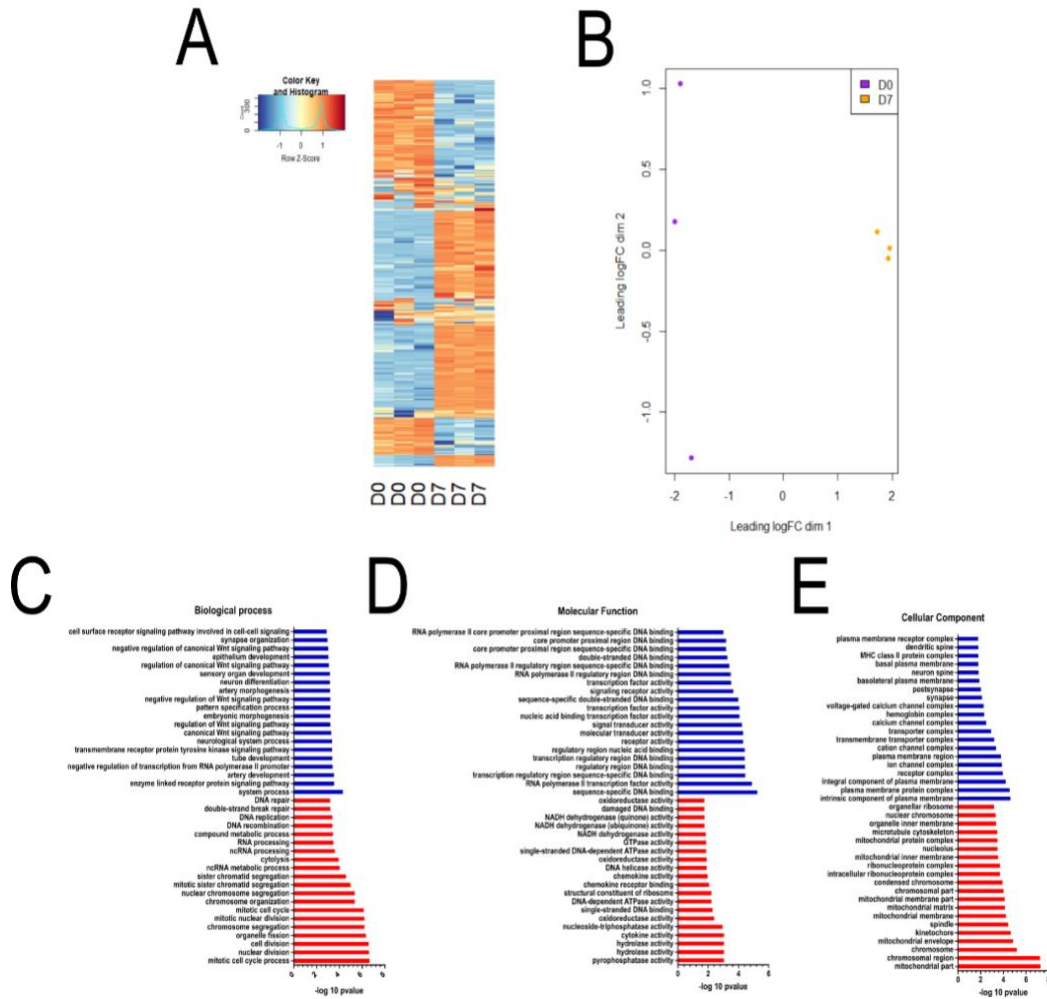


Figure 13. Gene enrichment and ontology analysis in response to PSA exposure. Gene ontology was conducted on differentially expressed genes (FDR>0.05 and log₂CPM>0). A) Heat map of top 500 differentially expressed (DE) genes on D7 compared to D0. B) Multidimensional scaling plot of all DE genes, showing scatter of D7 and D0 samples (each dot is a replicate sample). Top 20 significantly increased (red) or decreased (blue) gene ontology terms by C) Biological process D) Molecular Function and E) Cellular component. (values shown are -log₁₀ of p value)

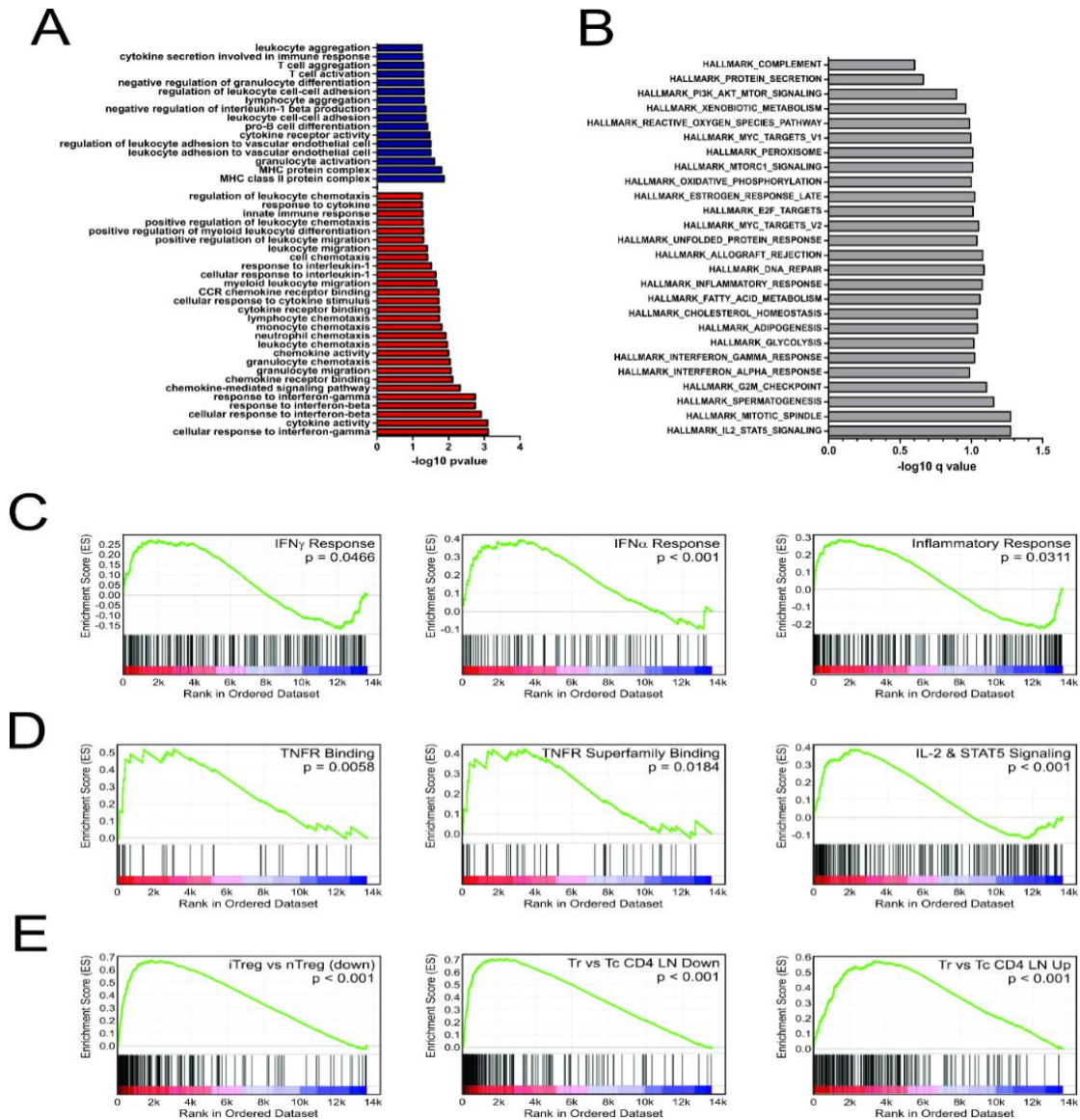


Figure 14. Gene set enrichment analysis of inflammatory and interferon related genes. Gene ontology and gene set enrichment analysis were conducted on differentially expressed genes (FDR>0.05 and log2CPM>0) A) Gene ontology analysis of differentially expressed genes increased (red) and decreased (blue) with PSA exposure in CD4⁺ T cells. GO terms with immunological relevance were extracted (44 terms). Gene ontology terms significantly associated ($P \leq 0.05$) were plotted as $-\log_{10}$ version. B) Hallmark gene set enrichment analysis of PSA stimulated cells. Gene sets significantly associated ($P \leq 0.05$) were plotted as $-\log_{10}$ of q value. GSEA analysis showing enrichment in C) IFN- γ , IFN- α and inflammatory response gene sets, D) TNF superfamily members and receptors, E) and gene sets associated with Treg functionality.

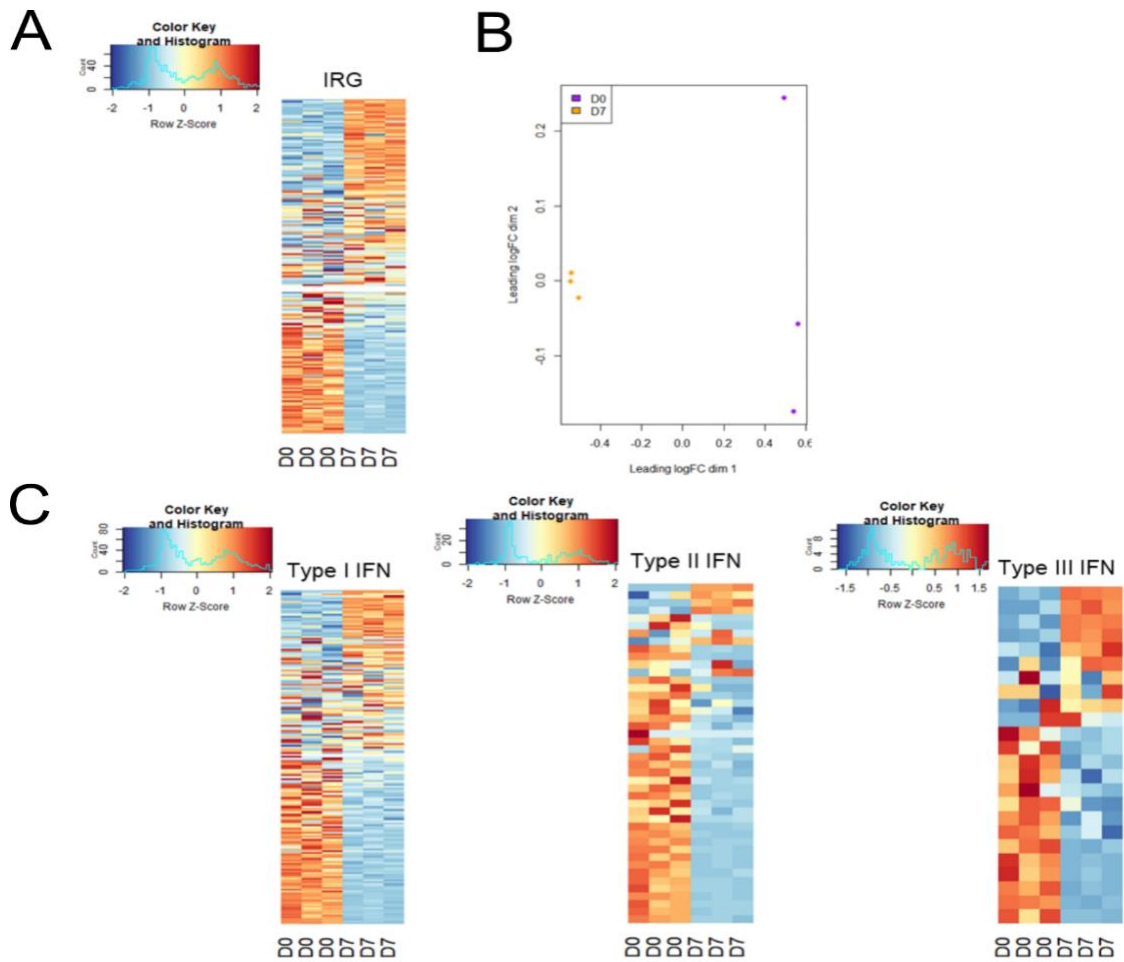


Figure 15. Gene expression IRG signature of PSA exposed cells. A) Heat map of interferon responsive genes from PSA exposed (D7) or unexposed (D0) CD4⁺ T cells. Values are row z-score. B) Multidimensional scatterplot of IRG data comparison of PSA exposed and non-exposed cells (D7 in orange, D0 in purple). C) Breakdown of IRG list into Type I, Type II or Type III IFN categories.

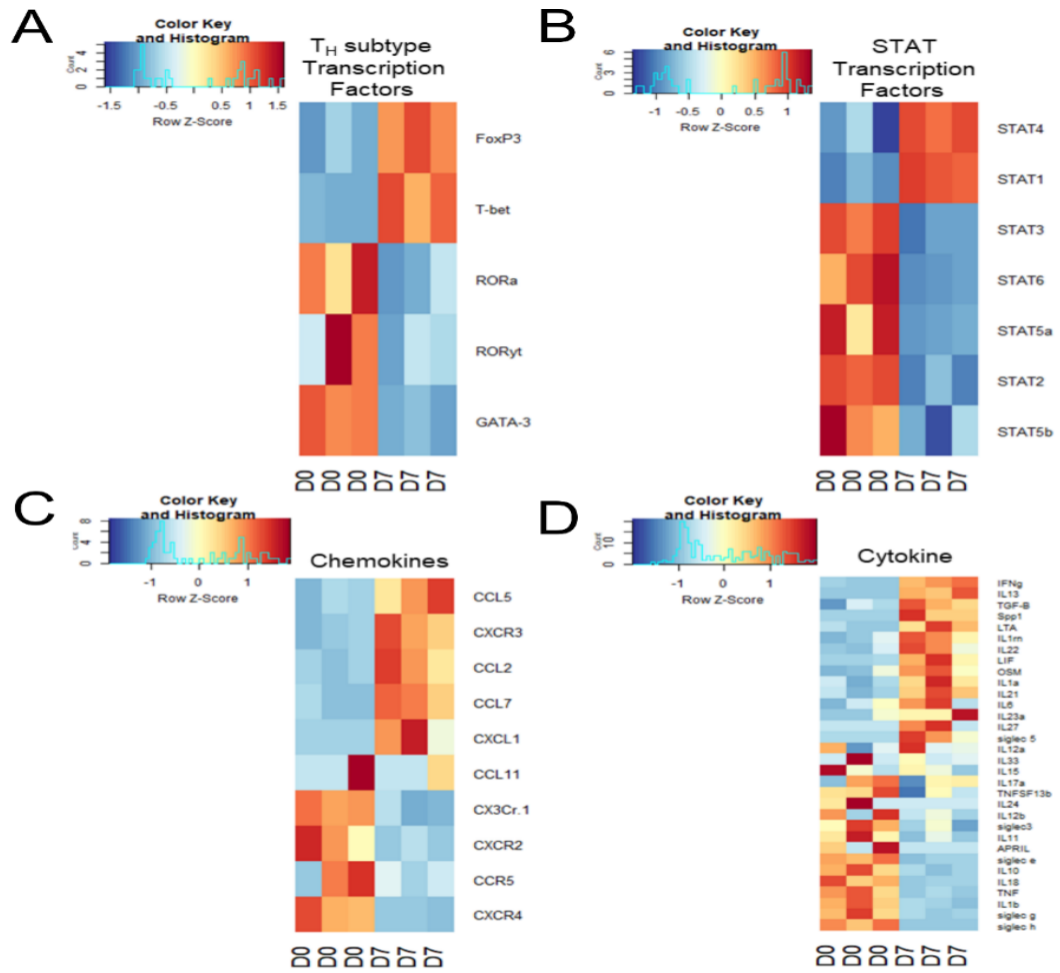


Figure 16. Transcription factor and signaling molecule profile of PSA exposed cells. Heat map of A) T subtype associated transcription factors B) STAT transcription factors C) Chemokines and D) Cytokines of PSA exposed T cells compared to control.

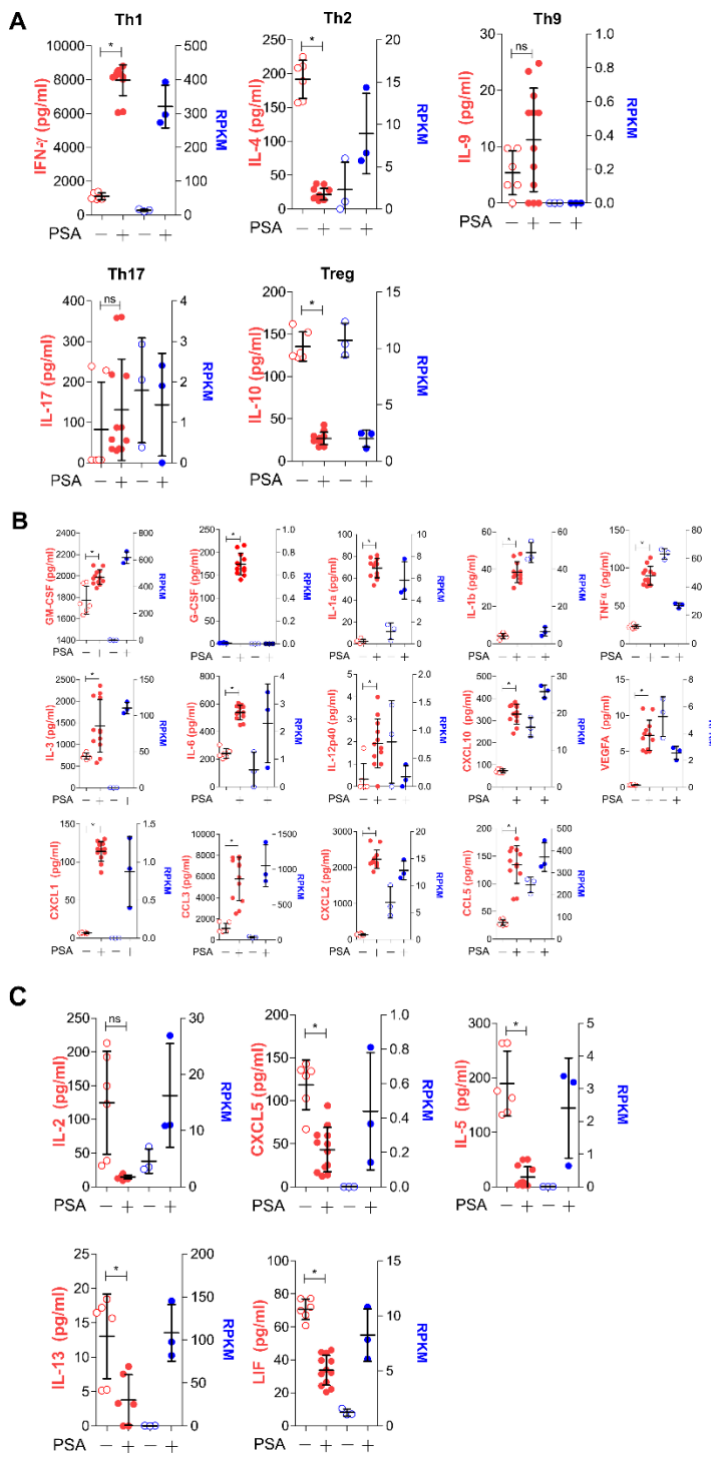


Figure 17. Secreted molecule profile of PSA exposed cells. Luminex analysis (Mouse Cytokine/Chemokine Array 32 plex) was used to determine secreted molecule profile of PSA exposed APC and T cell co-cultures after 7 days. Data shown reflects secreted proteins (left, red) and matching RNA-seq data (right, blue). A) T subtyped associated cytokines B) Molecules that significantly increased ($P \leq 0.05$) with PSA exposure. C) Molecules that significantly decreased ($P \leq 0.05$) with PSA exposure.

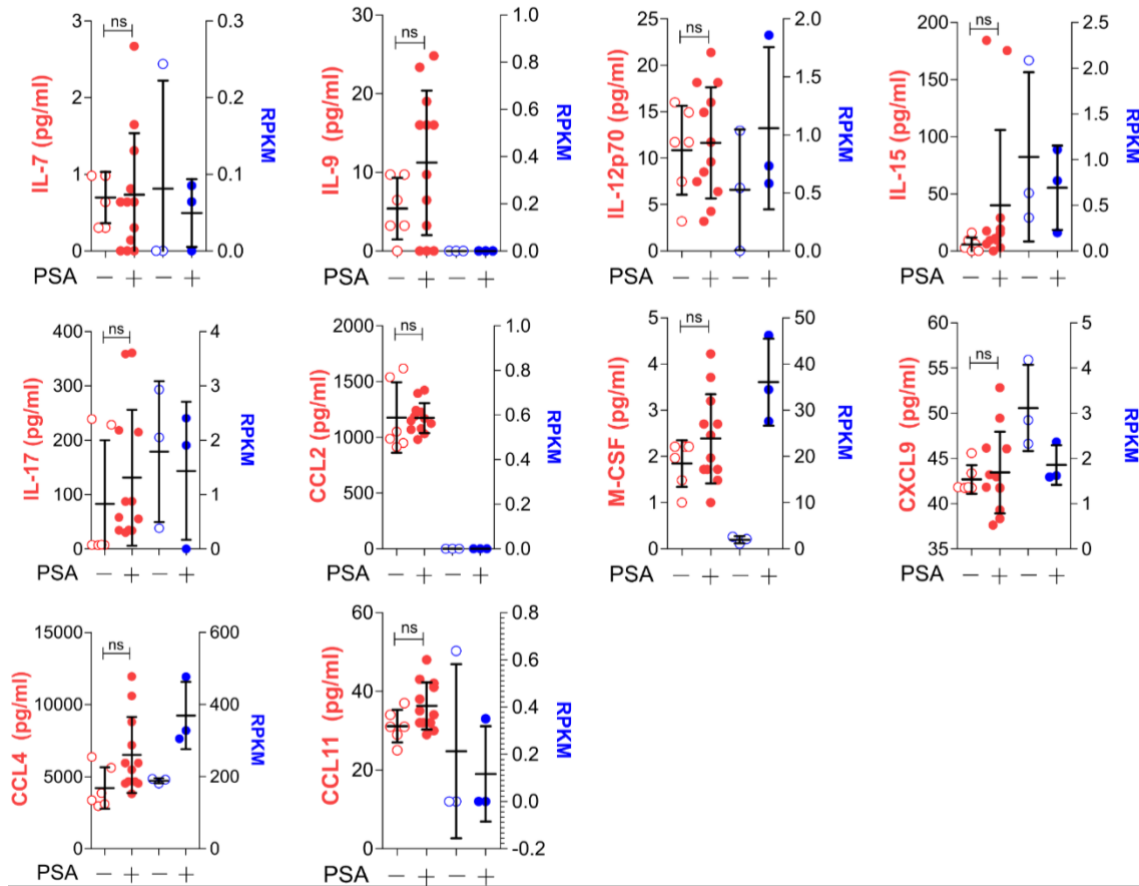


Figure 18. Unchanged cytokines and chemokines in PSA-exposed cell culture. Luminex and RNAseq values for cytokines and chemokines that are not impacted by PSA stimulation.

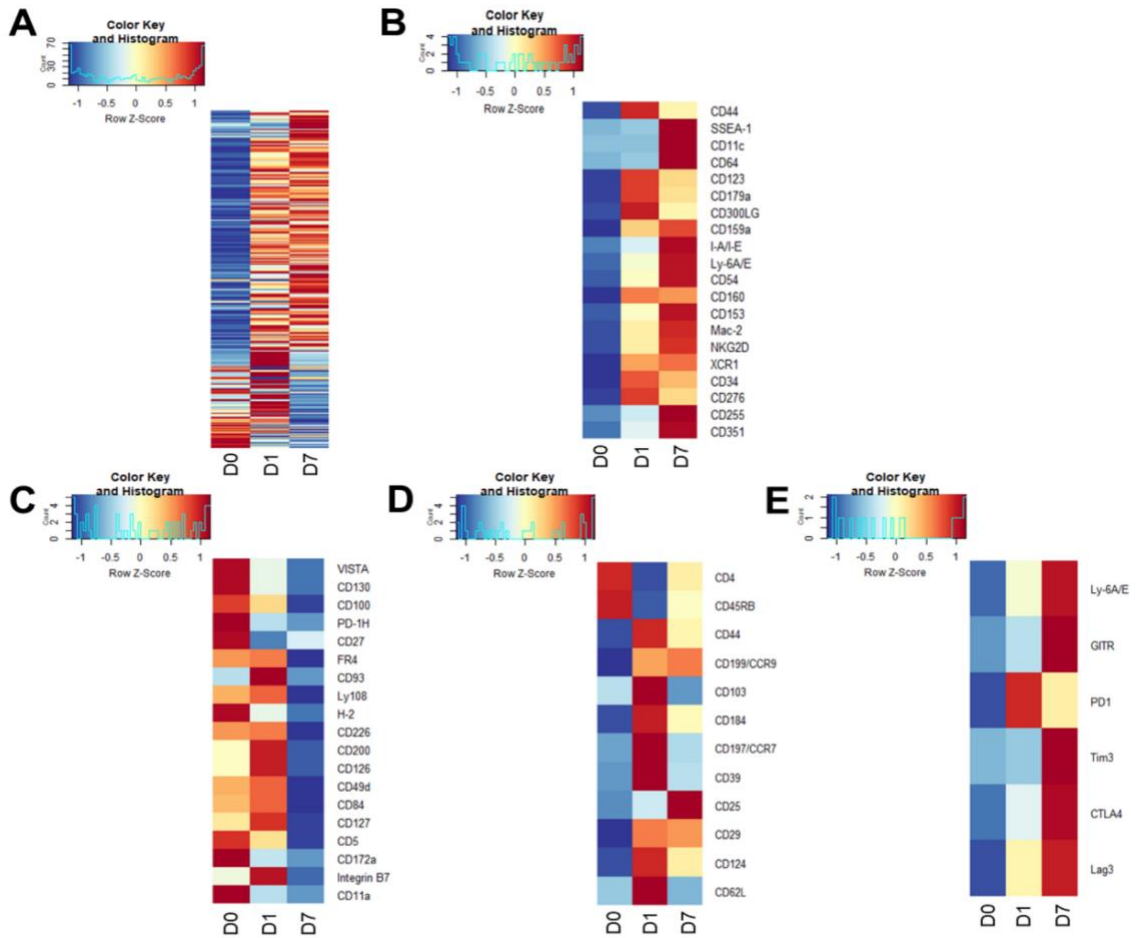


Figure 19. Cell surface marker expression of PSA exposed CD4⁺ T cells identifies immunomodulatory markers. High throughput flow cytometry was used to obtain the cell surface marker expression of 255 markers using LEGENDScreen Mouse PE kit. APC and T cells were co-cultured with PSA and collected at D0, D1 and D7. Data shown is geometric MFI from CD4⁺ T cells. Data is row z-scores. A) Summary heat map of all 255 markers on D0, D1 and D7. B) Top 20 markers most increased and C) decreased on D7 compared to D0. D) Markers previously used to identify PSA responsive T cells in human and murine experiments. E) Activation and immunomodulatory markers upregulated with PSA exposure.

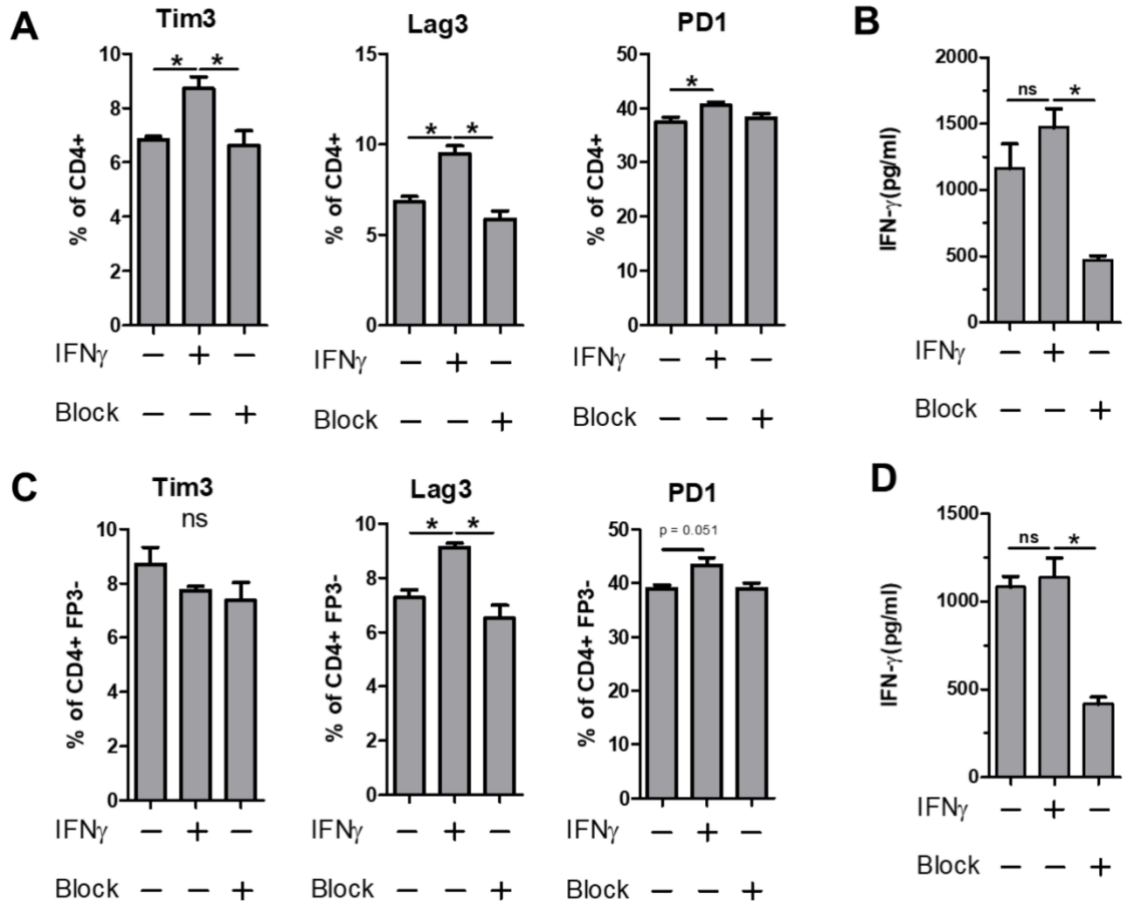


Figure 20. IFN- γ influence on immunomodulatory marker expression. Bulk or FP3⁻ CD4⁺ T cells were cultured *in vitro* for 3 days with α CD3 stimulation. Cells were supplemented with 10ng/ml of recombinant mouse IFN- γ or with 10 μ g/ml of α -IFN- γ blocking antibody. Marker expression assays with flow cytometry and culture supernatants were used for ELISA. Tim3, Lag3 and PD1 expression of A) Bulk or C) FP3⁻ CD4⁺ T cells with or without IFN or antibody blockade. ELISA data of culture supernatants from B) Bulk or D) FP3⁻ CD4⁺ T cell cultures. (significance of P \leq 0.05 = *)

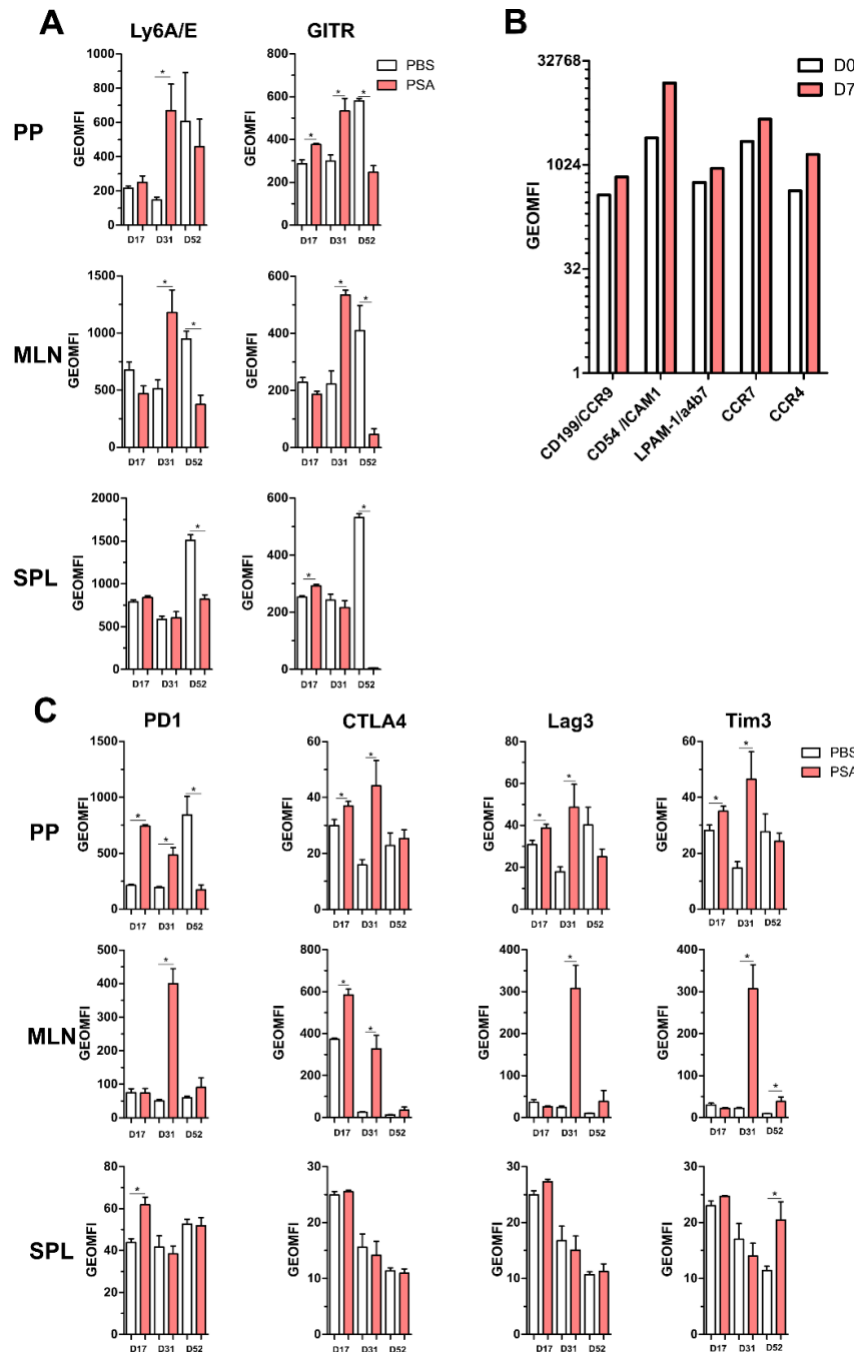


Figure 21. Gut associated lymphoid tissue enrichment of PSA induced markers. Mice were orally gavaged with 100µg of PSA dissolved in PBS every 72hrs, 5 gavages total. Peyer's patches, mesenteric lymph nodes and spleens were collected on D17, D31 or D52 after initial gavage. Data is geometric MFI. A) In vivo activation marker expression across organs and time points. B) Expression profile of immunomodulatory markers across organs and time points. (n=3 mice per group, significance of P≤0.05 = *)

Chapter 5 : Discussion and future directions

In the work presented in Chapter 3, we discovered a novel pathway of immune suppression mediated by the Rb^{Lo}Tem subset of regulatory T cells. We found that FoxP3⁺CD4⁺CD62L⁻CD44⁺CD45Rb^{Lo} effector/memory T cells (Rb^{Lo}Tem) coordinate a regulatory circuit in which they communicate with FoxP3⁺ Tregs to synergistically enhance IL-10 production, leading to the suppression of IFN γ and other cytokines *in vitro* and pulmonary inflammation *in vivo*. This pathway is mediated by a combination of IL-2 and IL-4 secreted by Rb^{Lo}Tem cells, leading to ligation of IL-4R α (CD124) on α CD3 ϵ -activated FoxP3⁺ Tregs and subsequent IL-10 production. The discovery of a novel T-effector cell-driven regulatory pathway and its underlying mechanism could have a major impact on how we understand the resolution of inflammation, the maintenance of homeostasis throughout the body, Treg behavior, and possibly how to control a variety of inflammatory diseases.

The collaboration between T cell subsets to favor a particular response is not a new concept. A recent example is the interaction between neuropilin-1 (Nrp1) and semaphorin-4a (Sema4a)[102]. Association of surface Sema4a on Tconv cells with Nrp1 on Tregs increased Treg survival and function *in vitro* and was found to be required for the *in vivo* suppression of inflammatory bowel disease. We found that the direct cell-to-cell contact via the Sema4a-Nrp1 axis does not account for the suppressive influence of Rb^{Lo}Tem cells on Tregs, as neutralization of Nrp1 with an antibody had no impact on *in vitro* IL-10 synergy. The data strongly support a contact-independent mechanism which relies upon soluble mediators, IL-2 and IL-4.

Since the establishment of the T_H1/T_H2 paradigm [139-141], it has been widely recognized that T_H1 responses oppose T_H2 responses, and vice versa, and that this is driven by key T_H1 or T_H2-associated cytokines. IL-4 has long been characterized as a central inducer of T_H2 cell development [142], a characteristic cytokine made by T_H2 cells [139-141], and a critical factor leading to the suppression of T_H1 cell differentiation [142-144]. T_H2 responses were originally described as including IL-4, IL-5, IL-6, and IL-10 [139-141]. As sophistication in the laboratory setting increased, IL-6 and IL-10 were removed from this general list, but it is pertinent to recall that IL-4 has been well documented to induce IL-10 production in T cells [145]. IL-4 has been linked to anti-inflammatory activity as far back as 1989 [146]. Human trials demonstrated that subcutaneous injection of psoriatic lesions with human IL-4 significantly reduced clinical scores [147], while IL-4 expression from a viral vector was able to prevent chondrocyte death and reduce cartilage erosion in a murine model of collagen-induced arthritis [148]. In EAE, gene delivery of IL-4 into mice selectively recruited FoxP3⁺CD25⁺ Tregs which eliminated the disease pathology [149]. IL-4 has also been implicated in the regulatory mechanisms required for the anti-inflammatory effects of intravenous immunoglobulin [150], and is known to be a robust driver of the wound healing phenotype of many macrophages, which includes IL-10 and TGF- β release [151, 152]. Indeed, IL-4 was previously shown to increase the suppressive capacity of CD25⁺ Tregs *in vitro* [153]. Although it is unclear why IL-4 was not depleted in our experiments (Fig 2) like IL-2 (Fig 1), it may be explained by differences in the relative rates of cytokine release by Rb^{L0}Tem cells and consumption by Tregs,

these findings not only show that IL-4 is a highly pleiotropic cytokine with a robust history of immune suppression, but they also strongly support the notion that Rb^{Lo}Tem cells could use IL-4 as a key driver of IL-10 and immune suppression under at least some inflammatory conditions.

In the work presented in Chapter 4, we used unbiased and complementary approaches to comprehensively characterize the T cell response to PSA in mice. Based on gene ontology analyses and in agreement with historical data on T cell proliferation in PSA responses [35], we found that PSA-responding T cells were highly metabolically active and proliferative through the upregulation of proteins involved in cell division and other key metabolic pathways. These T cells were dominated by an interferon-mediated expression profile, which matched the increased expression of Th1-associated transcription factors such as T-bet, STAT1 and STAT4. Increased secretion of TNF α , IL-6, and CXCL-10 are also consistent with a pro-inflammatory interferon-driven response.

Due to previous observations on the suppressive capacity of these cells, we sought potential mechanisms of immune inhibition. GSEA analyses revealed that PSA-responding T cells overall trend towards similarity with iTregs rather than conventional T cells. The genes that promote such a correlation included the regulatory T cell-associated transcription factor FoxP3. While our previously published data showed that this T cell communication to be dependent upon the release of IL-2 and IL-4 [118], we found that both IL-2 and IL-4 are upregulated transcriptionally, but are actually reduced in culture. One possibility is that these

cytokines are being removed from the media to support Tregs present within the bulk CD4⁺ T cell population used for these studies, similar to our prior findings [118]. This could explain both the divergence between mRNA and protein levels of IL-2 and IL-4 as well as the expansion of FoxP3 in these cultures, thereby supporting one model of PSA-mediated immune suppression where PSA-T cells directly support local Treg survival through cytokine release.

The PSA-responding T cells also expressed a host of co-regulatory receptors such as Tim3, Lag3 and PD-1. These molecules, also called immune checkpoints, have gained much attention due to their role in immune suppression in cancer. The expression of these inhibitory molecules both *in vitro* and within the GALT of PSA-exposed mice suggest that PSA-T cells also have a direct cell-to-cell mechanism of immune inhibition. These molecules also fit into an interferon-skewed response since we found that all three were increased at the cell surface of IFN γ -stimulated T cells.

We reveal the duality of the response through the characterization of an interferon-dominated expression profile, expression and use of Treg-supportive cytokines like IL-2 and IL-4, and the selective deployment of co-regulatory checkpoint receptors within the gut environment of PSA-exposed mice.

The work presented here has provided insight into the T cell based communication and profile after PSA exposure. Yet further work is required to validate and expand on the role of the molecules highlighted in Chapter 4.

This can be done by flow sorting PSA exposed cells using the immune checkpoints mentioned previously and test their efficacy in terms of suppressing or activating immune cells either by direct cell contact or by the secreted molecules they produce described above. Additionally, testing the role these PSA induced molecules play when interacting with Tregs. In cancer, it is well known that expression of immune checkpoints such as CTLA4 and PD-1 or their ligands is a tactic employed to effectively suppress the immune response and promote tumor survival. It is also known that tumors recruit Tregs for further protection[154]. Immune checkpoint blockade therapy also seems to interfere with tumor associated Tregs due to high expression of PD-1 and CTLA-4. Furthermore, some have reported a crucial role for PD-1 in the generation of peripheral Tregs[155]. So, it is possible that the expression of regulatory molecules via exposure to PSA is part of a recruitment and training mechanism for the maintenance of Tregs.

Yet there still remains the question concerning the antigen presenting cells responsible for the endocytosis and presentation of PSA to T cells. While the original presentation of PSA to T cells was demonstrated using DCs, it is possible that any MHCII⁺ cell is capable presenting PSA for T cell activation[34]. It has yet to be determined how the APCs change in response to PSA. One possibility is that APCs might play a supportive role by expressing complementary ligands to the immune checkpoints found on T cells in response to PSA. It has been demonstrated that regulatory DCs are able to upregulate expression of

immune checkpoints such as PD-1, increase expression of immunomodulatory cytokines TGF- β and IL-10, as well as generation of Tregs[156, 157]. The possibility remains that even though the T cell response might be the main mediator of the protection observed, perhaps the responding APCs might also play an important supportive role for the long term efficacy of the PSA response. Lastly, while the main focus of Chapter 4 centered around the strong IFN driven response and the molecules upregulated downstream, there is almost a guarantee that it is not the only mechanism engaged by PSA. There are still many avenues yet to be explored, in terms of prominent cytokines produced such as TNF α or IL-1 α , or expressed molecules not considered. Gene ontology highlighted a slew of categories that increased associated with B cell activation and chemotaxis which could be relevant in terms of the humoral response associated with PSA of which little is known. Similarly, we focused mainly on genes and markers that increased as a result of PSA, yet many cytokines and genes are downregulated as a direct response to PSA. This could also provide insight into what pathways need to be shut down in order for proper PSA activation to take place.

Overall, the work presented here illustrates a mechanism by which the microbiome is able to modulate the immune response by a commensal bacteria. The host-microbiome relationship has continued to evolve revealing its impacts in nearly all facets of human biology from nutrition to disease.

The upregulation of important immune regulatory markers and cytokines and expansion of Tem cells and in response to PSA is just one of the mechanisms

employed by the microbiome. Further work is necessary to understand the changes that occur not only in other immune cells such as APCs, but also in the tissue in which the microbes reside which has been shown to be important for proper colonization.

While more work is needed to understand the full impact of the microbiome, the work presented here gives a potential mechanism by which commensal bacteria native to the gut are able to support homeostasis locally and systemically.

References

1. Collins, F.S., M. Morgan, and A. Patrinos, *The Human Genome Project: Lessons from Large-Scale Biology*. Science, 2003. 300(5617): p. 286-290.
2. Legrain, P., et al., *The human proteome project: current state and future direction*. Molecular & cellular proteomics, 2011. 10(7).
3. Bradbury, J., *Human Epigenome Project—Up and Running*. PLOS Biology, 2003. 1(3): p. e82.
4. Brena, R.M., T.H.M. Huang, and C. Plass, *Toward a human epigenome*. Nature Genetics, 2006. 38(12): p. 1359-1360.
5. Turnbaugh, P.J., et al., *The Human Microbiome Project*. Nature, 2007. 449(7164): p. 804-810.
6. Shin, H., et al., *Changes in the Eye Microbiota Associated with Contact Lens Wearing*. mBio, 2016. 7(2): p. e00198-16.
7. Arumugam, M., et al., *Enterotypes of the human gut microbiome*. Nature, 2011. 473(7346): p. 174-180.
8. Grice, E.A. and J.A. Segre, *The skin microbiome*. Nature Reviews Microbiology, 2011. 9(4): p. 244-253.
9. Ma, B., L.J. Forney, and J. Ravel, *Vaginal Microbiome: Rethinking Health and Disease*. Annual Review of Microbiology, 2012. 66(1): p. 371-389.
10. Beck, J.M., V.B. Young, and G.B. Huffnagle, *The microbiome of the lung*. Translational Research, 2012. 160(4): p. 258-266.

11. Rosenfeld, J.A., C.E. Mason, and T.M. Smith, *Limitations of the human reference genome for personalized genomics*. PloS one, 2012. 7(7): p. e40294-e40294.
12. Bäckhed, F., et al., *Defining a healthy human gut microbiome: current concepts, future directions, and clinical applications*. Cell host & microbe, 2012. 12(5): p. 611-622.
13. Huttenhower, C., et al., *Structure, function and diversity of the healthy human microbiome*. Nature, 2012. 486(7402): p. 207-214.
14. Huttenhower, C., et al., *Structure, function and diversity of the healthy human microbiome*. nature, 2012. 486(7402): p. 207.
15. Shafquat, A., et al., *Functional and phylogenetic assembly of microbial communities in the human microbiome*. Trends in microbiology, 2014. 22(5): p. 261-266.
16. Grice, E.A., et al., *Topographical and temporal diversity of the human skin microbiome*. science, 2009. 324(5931): p. 1190-1192.
17. Douglas, C.A., et al., *DNA extraction approaches substantially influence the assessment of the human breast milk microbiome*. Scientific Reports, 2020. 10(1): p. 123.
18. Hunt, K.M., et al., *Characterization of the diversity and temporal stability of bacterial communities in human milk*. PloS one, 2011. 6(6): p. e21313.
19. Salter, S.J., et al., *Reagent and laboratory contamination can critically impact sequence-based microbiome analyses*. BMC biology, 2014. 12(1): p. 87.

20. Rajilić-Stojanović, M. and W.M. de Vos, *The first 1000 cultured species of the human gastrointestinal microbiota*. FEMS Microbiol Rev, 2014. 38(5): p. 996-1047.
21. Round, J.L., et al., *The Toll-like receptor 2 pathway establishes colonization by a commensal of the human microbiota*. Science, 2011. 332(6032): p. 974-977.
22. Shah, H.N. and S.E. Gharbia, *Ecological events in subgingival dental plaque with reference to bacteroides and fusobacterium species*. Infection, 1989. 17(4): p. 264-268.
23. Grice, E.A. and J.A. Segre, *Interaction of the microbiome with the innate immune response in chronic wounds*, in *Current topics in innate immunity II*. 2012, Springer. p. 55-68.
24. Aroutcheva, A., et al., *Defense factors of vaginal lactobacilli*. American journal of obstetrics and gynecology, 2001. 185(2): p. 375-379.
25. Faith, J.J., et al., *The long-term stability of the human gut microbiota*. Science, 2013. 341(6141).
26. Lozupone, C.A., et al., *Diversity, stability and resilience of the human gut microbiota*. Nature, 2012. 489(7415): p. 220-230.
27. Takeda, K., T. Kaisho, and S. Akira, *Toll-like receptors*. Annual review of immunology, 2003. 21(1): p. 335-376.
28. Rakoff-Nahoum, S., et al., *Recognition of commensal microflora by toll-like receptors is required for intestinal homeostasis*. Cell, 2004. 118(2): p. 229-241.

29. Slack, E., et al., *Innate and Adaptive Immunity Cooperate Flexibly to Maintain Host-Microbiota Mutualism*. *Science*, 2009. 325(5940): p. 617-620.
30. Bouskra, D., et al., *Lymphoid tissue genesis induced by commensals through NOD1 regulates intestinal homeostasis*. *Nature*, 2008. 456(7221): p. 507-510.
31. Iliev, I.D., et al., *Interactions between commensal fungi and the C-type lectin receptor Dectin-1 influence colitis*. *Science*, 2012. 336(6086): p. 1314-1317.
32. Shulzhenko, N., et al., *Crosstalk between B lymphocytes, microbiota and the intestinal epithelium governs immunity versus metabolism in the gut*. *Nature Medicine*, 2011. 17(12): p. 1585-1593.
33. Kawamoto, S., et al., *The Inhibitory Receptor PD-1 Regulates IgA Selection and Bacterial Composition in the Gut*. *Science*, 2012. 336(6080): p. 485-489.
34. Cobb, B.A., et al., *Polysaccharide processing and presentation by the MHCII pathway*. *Cell*, 2004. 117(5): p. 677-687.
35. Johnson, J.L., M.B. Jones, and B.A. Cobb, *Polysaccharide A from the capsule of Bacteroides fragilis induces clonal CD4+ T cell expansion*. *Journal of Biological Chemistry*, 2015. 290(8): p. 5007-5014.
36. Strachan, D.P., *Hay fever, hygiene, and household size*. *BMJ (Clinical research ed.)*, 1989. 299(6710): p. 1259-1260.

37. Ley, R.E., *Obesity and the human microbiome*. Current Opinion in Gastroenterology, 2010. 26(1): p. 5-11.
38. Kostic, A.D., et al., *The dynamics of the human infant gut microbiome in development and in progression toward type 1 diabetes*. Cell host & microbe, 2015. 17(2): p. 260-273.
39. Huttenhower, C., A.D. Kostic, and R.J. Xavier, *Inflammatory bowel disease as a model for translating the microbiome*. Immunity, 2014. 40(6): p. 843-854.
40. Kong, H.H., et al., *Temporal shifts in the skin microbiome associated with disease flares and treatment in children with atopic dermatitis*. Genome research, 2012. 22(5): p. 850-859.
41. Chen, J., et al., *Multiple sclerosis patients have a distinct gut microbiota compared to healthy controls*. Scientific reports, 2016. 6(1): p. 1-10.
42. Yatsunenko, T., et al., *Human gut microbiome viewed across age and geography*. nature, 2012. 486(7402): p. 222-227.
43. Stappenbeck, T.S. and H.W. Virgin, *Accounting for reciprocal host–microbiome interactions in experimental science*. Nature, 2016. 534(7606): p. 191-199.
44. Thaiss, C.A., et al., *Persistent microbiome alterations modulate the rate of post-dieting weight regain*. Nature, 2016. 540(7634): p. 544-551.
45. Costello, E.K., et al., *Bacterial Community Variation in Human Body Habitats Across Space and Time*. Science, 2009. 326(5960): p. 1694-1697.

46. Stecher, B., L. Maier, and W.-D. Hardt, *'Blooming' in the gut: how dysbiosis might contribute to pathogen evolution*. Nature Reviews Microbiology, 2013. 11(4): p. 277-284.
47. Langdon, A., N. Crook, and G. Dantas, *The effects of antibiotics on the microbiome throughout development and alternative approaches for therapeutic modulation*. Genome Medicine, 2016. 8(1): p. 39.
48. Francino, M.P., *Antibiotics and the Human Gut Microbiome: Dysbioses and Accumulation of Resistances*. Frontiers in Microbiology, 2016. 6(1543).
49. Sonnenburg, E.D., et al., *Diet-induced extinctions in the gut microbiota compound over generations*. Nature, 2016. 529(7585): p. 212-215.
50. Lupp, C., et al., *Host-mediated inflammation disrupts the intestinal microbiota and promotes the overgrowth of Enterobacteriaceae*. Cell host & microbe, 2007. 2(2): p. 119-129.
51. Stecher, B., et al., *Salmonella enterica Serovar Typhimurium Exploits Inflammation to Compete with the Intestinal Microbiota*. PLOS Biology, 2007. 5(10): p. e244.
52. Scagnolari, C., et al., *Role of interferons in chronic hepatitis C infection*. Current Drug Targets, 2017. 18(7): p. 844-850.
53. Teijaro, J.R., *Too much of a good thing: Sustained type 1 interferon signaling limits humoral responses to secondary viral infection*. European journal of immunology, 2016. 46(2): p. 300-302.

54. Wilson, E.B., et al., *Blockade of Chronic Type I Interferon Signaling to Control Persistent LCMV Infection*. *Science*, 2013. 340(6129): p. 202-207.
55. Cunningham, C.R., et al., *Type I and type II interferon coordinately regulate suppressive dendritic cell fate and function during viral persistence*. *PLoS pathogens*, 2016. 12(1): p. e1005356.
56. Honke, N., et al., *Immunoactivation induced by chronic viral infection inhibits viral replication and drives immunosuppression through sustained IFN-I responses*. *European journal of immunology*, 2016. 46(2): p. 372-380.
57. Abt, Michael C., et al., *Commensal Bacteria Calibrate the Activation Threshold of Innate Antiviral Immunity*. *Immunity*, 2012. 37(1): p. 158-170.
58. Gough, Daniel J., et al., *Constitutive Type I Interferon Modulates Homeostatic Balance through Tonic Signaling*. *Immunity*, 2012. 36(2): p. 166-174.
59. Tschurtschenthaler, M., et al., *Type I interferon signalling in the intestinal epithelium affects Paneth cells, microbial ecology and epithelial regeneration*. *Gut*, 2014. 63(12): p. 1921-1931.
60. Serena, G., et al., *Proinflammatory cytokine interferon- γ and microbiome-derived metabolites dictate epigenetic switch between forkhead box protein 3 isoforms in coeliac disease*. *Clinical & Experimental Immunology*, 2017. 187(3): p. 490-506.

61. Park, J., et al., *Short-chain fatty acids induce both effector and regulatory T cells by suppression of histone deacetylases and regulation of the mTOR–S6K pathway*. *Mucosal Immunology*, 2015. 8(1): p. 80-93.
62. Onderdonk, A.B., et al., *The capsular polysaccharide of Bacteroides fragilis as a virulence factor: comparison of the pathogenic potential of encapsulated and unencapsulated strains*. *Journal of Infectious Diseases*, 1977. 136(1): p. 82-89.
63. Polk, B.F. and D.L. Kasper, *Bacteroides fragilis Subspecies in Clinical Isolates*. *Annals of Internal Medicine*, 1977. 86(5): p. 569-571.
64. Baumann, H., et al., *Structural elucidation of two capsular polysaccharides from one strain of Bacteroides fragilis using high-resolution NMR spectroscopy*. *Biochemistry*, 1992. 31(16): p. 4081-4089.
65. Ochoa-Repáraz, J., et al., *A polysaccharide from the human commensal Bacteroides fragilis protects against CNS demyelinating disease*. *Mucosal Immunol*, 2010. 3(5): p. 487-95.
66. Mazmanian, S.K., J.L. Round, and D.L. Kasper, *A microbial symbiosis factor prevents intestinal inflammatory disease*. *Nature*, 2008. 453(7195): p. 620-5.
67. Johnson, J.L., M.B. Jones, and B.A. Cobb, *Bacterial capsular polysaccharide prevents the onset of asthma through T-cell activation*. *Glycobiology*, 2015. 25(4): p. 368-375.

68. Johnson, J.L., M.B. Jones, and B.A. Cobb, *Polysaccharide-experienced effector T cells induce IL-10 in FoxP3+ regulatory T cells to prevent pulmonary inflammation*. *Glycobiology*, 2018. 28(1): p. 50-58.
69. Falk, P.G., et al., *Creating and maintaining the gastrointestinal ecosystem: what we know and need to know from gnotobiology*. *Microbiol. Mol. Biol. Rev*, 1998. 62(4): p. 1157-1170.
70. Hooper, L.V., T. Midtvedt, and J.I. Gordon, *How host-microbial interactions shape the nutrient environment of the mammalian intestine*. *Annu. Rev. Nutr*, 2002. 22: p. 283-307.
71. Nishio, J. and K. Honda, *Immunoregulation by the gut microbiota*. *Cell Mol. Life Sci*, 2012. 69(21): p. 3635-3650.
72. Peterson, C.T., et al., *Immune homeostasis, dysbiosis and therapeutic modulation of the gut microbiota*. *Clin. Exp. Immunol*, 2015. 179(3): p. 363-377.
73. Johnson, J.L., M.B. Jones, and B.A. Cobb, *Polysaccharide-Experienced Effector T cells Induce IL-10 in FoxP3+ Regulatory T cells to Prevent Pulmonary Inflammation*. *Glycobiology*, 2017.
74. Mazmanian, S.K., J.L. Round, and D.L. Kasper, *A microbial symbiosis factor prevents intestinal inflammatory disease*. *Nature*, 2008. 453(7195): p. 620-625.
75. Ochoa-Reparaz, J., et al., *A polysaccharide from the human commensal Bacteroides fragilis protects against CNS demyelinating disease*. *Mucosal. Immunol*, 2010. 3(5): p. 487-495.

76. Tzianabos, A.O., et al., *Structural features of polysaccharides that induce intra-abdominal abscesses*. Science, 1993. 262(5132): p. 416-419.
77. Krinos, C.M., et al., *Extensive surface diversity of a commensal microorganism by multiple DNA inversions*. Nature, 2001. 414(6863): p. 555-558.
78. Tzianabos, A.O., et al., *The capsular polysaccharide of Bacteroides fragilis comprises two ionically linked polysaccharides*. J. Biol. Chem, 1992. 267(25): p. 18230-18235.
79. Johnson, J.L., M.B. Jones, and B.A. Cobb, *Polysaccharide A from the capsule of Bacteroides fragilis induces clonal CD4+ T cell expansion*. J. Biol. Chem, 2015. 290(8): p. 5007-5014.
80. Tzianabos, A.O., et al., *Structural characterization of two surface polysaccharides of Bacteroides fragilis*. Trans. Assoc. Am. Physicians, 1991. 104: p. 285-295.
81. Kreisman, L.S., et al., *Structure and function relations with a T-cell-activating polysaccharide antigen using circular dichroism*. Glycobiology, 2007. 17(1): p. 46-55.
82. Cobb, B.A. and D.L. Kasper, *Characteristics of carbohydrate antigen binding to the presentation protein HLA-DR*. Glycobiology, 2008. 18(9): p. 707-718.
83. Shevach, E.M., *Foxp3(+) T Regulatory Cells: Still Many Unanswered Questions-A Perspective After 20 Years of Study*. Front Immunol, 2018. 9: p. 1048.

84. Sakaguchi, S., et al., *The plasticity and stability of regulatory T cells*. Nat Rev Immunol, 2013. 13(6): p. 461-7.
85. Rudensky, A.Y., *Regulatory T cells and Foxp3*. Immunol Rev, 2011. 241(1): p. 260-8.
86. Battaglia, M., et al., *Tr1 cells: From discovery to their clinical application*. Seminars in Immunology, 2006. 18(2): p. 120-127.
87. Roncarolo, M.G., et al., *Interleukin-10-secreting type 1 regulatory T cells in rodents and humans*. Immunol Rev, 2006. 212: p. 28-50.
88. Morrissey, P.J. and K. Charrier, *Induction of wasting disease in SCID mice by the transfer of normal CD4⁺/CD45RB^{hi} T cells and the regulation of this autoreactivity by CD4⁺/CD45RB^{lo} T cells*. Res Immunol, 1994. 145(5): p. 357-62.
89. Shimada, A., et al., *Immune regulation in type 1 diabetes*. J Autoimmun, 1996. 9(2): p. 263-9.
90. Smart, V., et al., *A plant-based allergy vaccine suppresses experimental asthma via an IFN-gamma and CD4⁺CD45RB^{low} T cell-dependent mechanism*. J Immunol, 2003. 171(4): p. 2116-26.
91. Ruiz-Perez, B., et al., *Modulation of surgical fibrosis by microbial zwitterionic polysaccharides*. Proc Natl Acad Sci U S A, 2005. 102(46): p. 16753-8.
92. Johnson, J.L., M.B. Jones, and B.A. Cobb, *Polysaccharide A from the capsule of Bacteroides fragilis induces clonal CD4⁺ T cell expansion*. J Biol Chem, 2015. 290(8): p. 5007-14.

93. Kamanaka, M., et al., *Memory/effector (CD45RB(lo)) CD4 T cells are controlled directly by IL-10 and cause IL-22-dependent intestinal pathology*. J Exp Med, 2011. 208(5): p. 1027-40.
94. Asseman, C., et al., *An essential role for interleukin 10 in the function of regulatory T cells that inhibit intestinal inflammation*. J Exp Med, 1999. 190(7): p. 995-1004.
95. Kreisman, L.S. and B.A. Cobb, *Glycoantigens induce human peripheral Tr1 cell differentiation with gut-homing specialization*. J Biol Chem, 2011. 286(11): p. 8810-8.
96. Johnson, J.R., et al., *Continuous exposure to house dust mite elicits chronic airway inflammation and structural remodeling*. Am J Respir Crit Care Med, 2004. 169(3): p. 378-85.
97. Bolger, A.M., M. Lohse, and B. Usadel, *Trimmomatic: a flexible trimmer for Illumina sequence data*. Bioinformatics, 2014. 30(15): p. 2114-20.
98. Kim, D., et al., *TopHat2: accurate alignment of transcriptomes in the presence of insertions, deletions and gene fusions*. Genome Biol, 2013. 14(4): p. R36.
99. Frankish, A., et al., *Comparison of GENCODE and RefSeq gene annotation and the impact of reference geneset on variant effect prediction*. BMC Genomics, 2015. 16 Suppl 8: p. S2.
100. Anders, S., P.T. Pyl, and W. Huber, *HTSeq-a Python framework to work with high-throughput sequencing data*. Bioinformatics, 2015. 31(2): p. 166-169.

101. Love, M.I., W. Huber, and S. Anders, *Moderated estimation of fold change and dispersion for RNA-seq data with DESeq2*. *Genome Biol*, 2014. 15(12): p. 550.
102. Delgoffe, G.M., et al., *Stability and function of regulatory T cells is maintained by a neuropilin-1-semaphorin-4a axis*. *Nature*, 2013. 501(7466): p. 252-+.
103. Arenas-Ramirez, N., J. Woytschak, and O. Boyman, *Interleukin-2: Biology, Design and Application*. *Trends Immunol*, 2015. 36(12): p. 763-777.
104. Hevia, A., et al., *Intestinal Dysbiosis Associated with Systemic Lupus Erythematosus*. *mBio*, 2014. 5(5): p. e01548-14.
105. Shamriz, O., et al., *Microbiota at the crossroads of autoimmunity*. *Autoimmunity reviews*, 2016. 15(9): p. 859-869.
106. Bisgaard, H., et al., *Reduced diversity of the intestinal microbiota during infancy is associated with increased risk of allergic disease at school age*. *Journal of Allergy and Clinical Immunology*, 2011. 128(3): p. 646-652. e5.
107. Roy, S. and G. Trinchieri, *Microbiota: a key orchestrator of cancer therapy*. *Nature Reviews Cancer*, 2017. 17(5): p. 271.
108. Dzutsev, A., et al., *The role of the microbiota in inflammation, carcinogenesis, and cancer therapy*. *European journal of immunology*, 2015. 45(1): p. 17-31.
109. Sofi, M.H., et al., *Polysaccharide A–Dependent Opposing Effects of Mucosal and Systemic Exposures to Human Gut Commensal Bacteroides fragilis in Type 1 Diabetes*. *Diabetes*, 2019. 68(10): p. 1975-1989.

110. Ochoa-Reparaz, J., et al., *A polysaccharide from the human commensal Bacteroides fragilis protects against CNS demyelinating disease*. Mucosal immunology, 2010. 3(5): p. 487-495.
111. Erturk-Hasdemir, D. and D.L. Kasper, *Finding a needle in a haystack: Bacteroides fragilis polysaccharide A as the archetypical symbiosis factor*. Annals of the New York Academy of Sciences, 2018. 1417(1): p. 116-129.
112. Troy, E.B. and D.L. Kasper, *Beneficial effects of Bacteroides fragilis polysaccharides on the immune system*. Frontiers in bioscience: a journal and virtual library, 2010. 15: p. 25.
113. Gibson, F.C., et al., *Cellular mechanism of intraabdominal abscess formation by Bacteroides fragilis*. The Journal of Immunology, 1998. 160(10): p. 5000-5006.
114. Wang , Q., et al., *A bacterial carbohydrate links innate and adaptive responses through Toll-like receptor 2*. Journal of Experimental Medicine, 2006. 203(13): p. 2853-2863.
115. Ryan, S.O., et al., *MHCII glycosylation modulates Bacteroides fragilis carbohydrate antigen presentation*. Journal of Experimental Medicine, 2011. 208(5): p. 1041-1053.
116. Tzianabos, A.O., et al., *Polysaccharide-mediated protection against abscess formation in experimental intra-abdominal sepsis*. The Journal of clinical investigation, 1995. 96(6): p. 2727-2731.

117. Chung, D.R., et al., *CD4+ T cells regulate surgical and postinfectious adhesion formation*. The Journal of experimental medicine, 2002. 195(11): p. 1471-1478.
118. Jones, M.B., et al., *CD45Rb-low effector T cells require IL-4 to induce IL-10 in FoxP3 Tregs and to protect mice from inflammation*. PloS one, 2019. 14(5).
119. Schroder, K., et al., *Interferon- γ : an overview of signals, mechanisms and functions*. Journal of Leukocyte Biology, 2004. 75(2): p. 163-189.
120. Lawless, V.A., et al., *Stat4 regulates multiple components of IFN- γ -inducing signaling pathways*. The Journal of Immunology, 2000. 165(12): p. 6803-6808.
121. Ramakrishna, C., et al., *Bacteroides fragilis polysaccharide a induces IL-10 secreting B and T cells that prevent viral encephalitis*. Nature communications, 2019. 10(1): p. 1-13.
122. Alvarez, C.A. and B.A. Cobb, *Purification of Capsular Polysaccharide Complex from Gram-Negative Bacteria*, in *Bacterial Polysaccharides: Methods and Protocols*, I. Brockhausen, Editor. 2019, Springer New York: New York, NY. p. 25-35.
123. Subramanian, A., et al., *Gene set enrichment analysis: A knowledge-based approach for interpreting genome-wide expression profiles*. Proceedings of the National Academy of Sciences, 2005. 102(43): p. 15545-15550.

124. Liberzon, A., et al., *Molecular signatures database (MSigDB) 3.0*. Bioinformatics, 2011. 27(12): p. 1739-1740.
125. Qing, Y. and G.R. Stark, *Alternative activation of STAT1 and STAT3 in response to interferon- γ* . Journal of Biological Chemistry, 2004. 279(40): p. 41679-41685.
126. Schneider, W.M., M.D. Chevillotte, and C.M. Rice, *Interferon-stimulated genes: a complex web of host defenses*. Annual review of immunology, 2014. 32: p. 513-545.
127. García-Sastre, A. and C.A. Biron, *Type 1 interferons and the virus-host relationship: a lesson in detente*. Science, 2006. 312(5775): p. 879-882.
128. Donnelly, R.P. and S.V. Kotenko, *Interferon-lambda: a new addition to an old family*. Journal of Interferon & Cytokine Research, 2010. 30(8): p. 555-564.
129. Vogel, C. and E.M. Marcotte, *Insights into the regulation of protein abundance from proteomic and transcriptomic analyses*. Nature reviews genetics, 2012. 13(4): p. 227-232.
130. DeLong, J.H., et al., *Cytokine- and TCR-Mediated Regulation of T Cell Expression of Ly6C and Sca-1*. The Journal of Immunology, 2018. 200(5): p. 1761-1770.
131. Shimizu, Y., et al., *Dual role of the CD44 molecule in T cell adhesion and activation*. The Journal of Immunology, 1989. 143(8): p. 2457-2463.

132. Nakayama, M., et al., *Involvement of Tweak in Interferon γ -Stimulated Monocyte Cytotoxicity*. Journal of Experimental Medicine, 2000. 192(9): p. 1373-1380.
133. Delaire, S., et al., *CD100 is a leukocyte semaphorin*. Cellular and Molecular Life Sciences CMLS, 1998. 54(11): p. 1265-1276.
134. Hendriks, J., et al., *CD27 is required for generation and long-term maintenance of T cell immunity*. Nature Immunology, 2000. 1(5): p. 433-440.
135. Freeman, G.J., et al., *Engagement of the Pd-1 Immunoinhibitory Receptor by a Novel B7 Family Member Leads to Negative Regulation of Lymphocyte Activation*. Journal of Experimental Medicine, 2000. 192(7): p. 1027-1034.
136. Riley, J.L., *PD-1 signaling in primary T cells*. Immunological Reviews, 2009. 229(1): p. 114-125.
137. Anderson, A.C., N. Joller, and V.K. Kuchroo, *Lag-3, Tim-3, and TIGIT: co-inhibitory receptors with specialized functions in immune regulation*. Immunity, 2016. 44(5): p. 989-1004.
138. Woo, S.-R., et al., *Immune Inhibitory Molecules LAG-3 and PD-1 Synergistically Regulate T-cell Function to Promote Tumoral Immune Escape*. Cancer Research, 2012. 72(4): p. 917-927.
139. Mosmann, T.R., *Regulation of immune responses by T cells with different cytokine secretion phenotypes: role of a new cytokine, cytokine synthesis*

- inhibitory factor (IL 10)*. Int Arch Allergy Appl Immunol, 1991. 94(1-4): p. 110-5.
140. Mosmann, T.R., et al., *Two types of murine helper T cell clone. I. Definition according to profiles of lymphokine activities and secreted proteins*. J Immunol, 1986. 136(7): p. 2348-57.
141. Mosmann, T.R. and R.L. Coffman, *TH1 and TH2 cells: different patterns of lymphokine secretion lead to different functional properties*. Annu Rev Immunol, 1989. 7: p. 145-73.
142. Akdis, M., et al., *Interleukins, from 1 to 37, and interferon-gamma: receptors, functions, and roles in diseases*. J Allergy Clin Immunol, 2011. 127(3): p. 701-21 e1-70.
143. Janeway, C.A., et al., *Immunobiology: The Immune System in Health & Disease*. 6th edition ed. 2005, Hamden, CT: Garland Publishing.
144. Mak, T.W., M.E. Saunders, and B.D. Jett, *Primer to the Immune Response*. 2 ed. 2013: Newnes.
145. Chang, H.D., et al., *Expression of IL-10 in Th memory lymphocytes is conditional on IL-12 or IL-4, unless the IL-10 gene is imprinted by GATA-3*. European Journal of Immunology, 2007. 37(3): p. 807-817.
146. Hart, P.H., et al., *Potential antiinflammatory effects of interleukin 4: suppression of human monocyte tumor necrosis factor alpha, interleukin 1, and prostaglandin E2*. Proc Natl Acad Sci U S A, 1989. 86(10): p. 3803-7.

147. Ghoreschi, K., et al., *Interleukin-4 therapy of psoriasis induces Th2 responses and improves human autoimmune disease*. Nat Med, 2003. 9(1): p. 40-6.
148. Lubberts, E., et al., *Adenoviral vector-mediated overexpression of IL-4 in the knee joint of mice with collagen-induced arthritis prevents cartilage destruction*. J Immunol, 1999. 163(8): p. 4546-56.
149. Butti, E., et al., *IL4 gene delivery to the CNS recruits regulatory T cells and induces clinical recovery in mouse models of multiple sclerosis*. Gene Ther, 2008. 15(7): p. 504-15.
150. Anthony, R.M., et al., *Intravenous gammaglobulin suppresses inflammation through a novel T(H)2 pathway*. Nature, 2011. 475(7354): p. 110-U133.
151. Gordon, S., *Alternative activation of macrophages*. Nat Rev Immunol, 2003. 3(1): p. 23-35.
152. Ponomarev, E.D., et al., *CNS-Derived interleukin-4 is essential for the regulation of autoimmune inflammation and induces a state of alternative activation in microglial cells*. Journal of Neuroscience, 2007. 27(40): p. 10714-10721.
153. Maerten, P., et al., *Effects of interleukin 4 on CD25+CD4+ regulatory T cell function*. J Autoimmun, 2005. 25(2): p. 112-20.
154. Sasidharan Nair, V. and E. Elkord, *Immune checkpoint inhibitors in cancer therapy: a focus on T-regulatory cells*. Immunology & Cell Biology, 2018. 96(1): p. 21-33.

155. Chen, X., et al., *PD-1 regulates extrathymic regulatory T-cell differentiation*. European journal of immunology, 2014. 44(9): p. 2603-2616.
156. Morelli, A.E. and A.W. Thomson, *Tolerogenic dendritic cells and the quest for transplant tolerance*. Nature Reviews Immunology, 2007. 7(8): p. 610-621.
157. Manicassamy, S. and B. Pulendran, *Dendritic cell control of tolerogenic responses*. Immunological reviews, 2011. 241(1): p. 206-227.